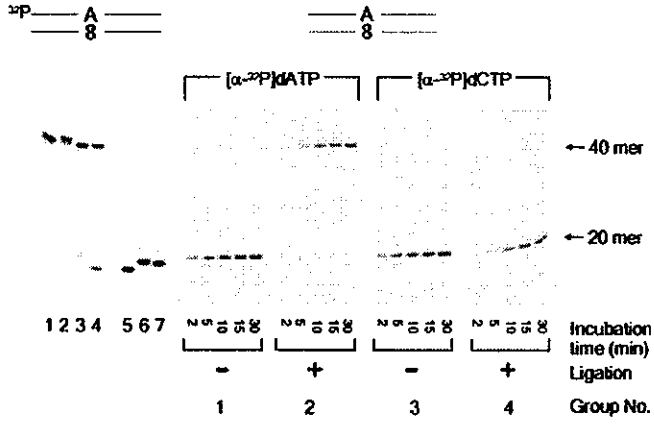

Figure 6. Reconstitution of MYH-initiated short-patch BER. Substrate DNA (duplex 40mer) is shown above the panel. Lanes 1–4 show base excision reaction catalyzed by MYH, using 5′-^{32}P-labeled substrate. Lane 1, substrate DNA; lanes 2 and 3, incubated with 10 nM MYH for 30 min (lane 2) followed by heating at 90°C for 3 min (lane 3); lane 4, incubated with MYH followed by APE1 treatment for 30 min in the presence of 150 mM KCl; lane 5, 5′-^{32}P-labeled standard 19mer corresponding to MYH/APE1-generated product; lanes 6 and 7, standard 19mer plus 3′-dA (lane 6) or 3′-dC (lane 7). All the other lanes show reconstitution reaction using [α-^{32}P]dATP or [α-^{32}P]dCTP in the presence or in the absence of ligation reaction catalyzed by DNA ligase IIIα/XRCC1.

examined, and no significant effects were observed (data not shown). The ligation catalyzed by DNA ligase I was also characterized under the same condition. Both in the presence and in the absence of 150 mM KCl, ligation of a 3′-dA terminus was more efficient than that of a dC terminus pairing to 8-oxo-dG, which was similar to the result with ligase IIIα, but the difference was less marked. We have also tested *E.coli* and T4 DNA ligases, and the results were similar to those with ligase I (data not shown). From these results, it is concluded that DNA ligases, especially human ligase IIIα, are much more active on a dA terminus than on a dC terminus pairing to 8-oxo-dG.

Adenine base excision and strand incision catalyzed by MYH and APE1

When 5′-^{32}P labeled 40mer duplex bearing a dA:8-oxo-dG pair was incubated with MYH, a faint band migrating above 19mer was detected (Figure 5). This band may be the product of β-elimination reaction of an AP site generated by MYH. When APE1 was added to this reaction mixture in the presence of 150 m KCl, a distinct band was generated. This band corresponds to 19mer with 3′-OH terminus. Thus, the combined action of MYH and APE1 generates a 1 nt gap opposite 8-oxo-dG with 3′-OH and 5′dRP termini.

Reconstitution of MYH-initiated short-patch BER of dA:8-oxo-dG mispair

So far, each step of short-patch BER was characterized individually. In this section, short-patch BER was reconstituted using purified proteins. As described in 'Materials and Methods', unlabeled duplex 40mer was first incubated with MYH, then the reaction mixture was supplemented with the other protein factors (APE1, pol β and DNA ligase IIIα/XRCC1) and co-factors (KCl, ATP, dATP, dCTP and [α-^{32}P] dATP or [α-^{32}P] dCTP). The dA (group 1) and dC (group 3) were inserted opposite 8-oxo-dG as revealed in reaction mixtures lacking the ligase (Figure 6). Although inserted dA was ligated efficiently (group 2), dC was not (group 4). These results indicate that the short-patch repair is completed only when dAMP is inserted opposite 8-oxo-dG.

DISCUSSION

8-Oxo-dG exerts its genotoxity mainly by pairing with dA during DNA replication. In *E.coli*, the frequency of this misincorporation is ~30% when measured in *mutM*$^-$*mutY*$^-$ cells, and more than 90% of these misincorporated dAs are removed by MutY-initiated post-replication repair (22). Although a misincorporation frequency of dA has not yet been determined in human cells, a similar repair process is expected to operate since MYH-defective cells are mutation-prone (9).

In this paper, we conducted biochemical studies using purified proteins to understand the mammalian post-replication repair. We focused on the short-patch BER and examined characteristics of enzymes involved in this repair. None of the mammalian DNA polymerases examined inserted exclusively dC opposite 8-oxo-dG, and mis-inserted dA was not specifically proofread by human APE1. However, at a ligation step, human DNA ligases I and III ligated a 3′-dA terminus pairing to 8-oxo-dG much more efficiently than a 3′-dC terminus. Thus, the ligation step discriminates dA from dC. In reconstitution experiments, DNA was ligated only when dA was inserted opposite 8-oxo-dG, indicating that MYH-initiated short-patch BER is futile and a dC:8-oxo-dG pair must proceed to long-patch BER to complete the repair. Our results support the previous suggestion that the long-patch pathway is responsible for this repair (12,15,16). One of the major questions about the repair of a dA:8-oxo-dG mispair is which DNA polymerase is responsible for dC insertion opposite 8-oxo-dG. In the experiments with cell extracts (15), the gap-filling synthesis step is sensitive to aphidicolin, suggesting that a replicative polymerase, pol δ/pol ε, is critical. However, it is unknown whether the aphidicolin-sensitive polymerase catalyzes both nucleotide insertion opposite 8-oxo-dG and extension. Indeed, there is a suggestion that pol β and pol δ/ε play a role in nucleotide insertion and extension steps, respectively, during a long-patch repair (23,24). Therefore, it is possible that nucleotide insertion opposite 8-oxo-dG and extension from the terminus are catalyzed by different polymerases. Furthermore, there are conflicting reports on the sensitivity of pol λ to aphidicolin (25,26). Since this polymerase possesses dRPase activity (27), it may function in short-patch BER. Therefore, we assessed mammalian DNA polymerases for their abilities to insert a nucleotide opposite 8-oxo-dG, using a gapped substrate. A widely spread idea is that 'repair' DNA polymerase preferentially inserts dC opposite 8-oxo-dG. However, none of the DNA polymerases examined exclusively inserted dC. The dRPase activity is required to complete short-patch BER. Pol β (28) and pol λ (27) have dRPase activities while the activity of pol ι is controversial (29,30). Pol β and pol λ, members of X-family polymerases, efficiently inserted both dA and dC into a 1 nt gap opposite 8-oxo-dG (Figure 1). Thus,

both enzymes are candidate DNA polymerases involved in this BER. Although pol η preferentially inserted dC, it is reported that pol η, pol κ and pol ι are covalently trapped by a 5′-dRP residue and their repair synthesis activities are greatly reduced (30). In addition, pol ι or pol κ is not very active in inserting a nucleotide opposite 8-oxo-dG. Thus, these polymerases may not be suitable for the repair synthesis. Pol δ also can insert dC and dA opposite the lesion as reported previously (31) and may be responsible for both steps. It is conceivable that a certain factor keeps 8-oxo-dG in the *anti* conformation and assists DNA polymerase to insert dC opposite 8-oxo-dG (32). However, whichever the polymerase that is responsible for the dC insertion is, short-patch BER cannot complete the post-replication repair since a dC terminus is not ligated efficiently by DNA ligases, especially by ligase III/XRCC1 that is believed to be involved in short-patch BER (6).

Our results support the previous idea that the long-patch repair is responsible for this post-replicaton repair (12,15,16). This pathway may be selected at the initiation of the repair since proteins necessary for the long-patch repair, such as MYH, PCNA, FEN1 and pol δ, are immediately available in the replication foci (11). Alternatively, it can be the result of the inhibition of short-patch repair as shown here. These two possibilities may be distinguished by identifying a polymerase that catalyzes nucleotide insertion opposite 8-oxo-dG. The possible *in vivo* roles for pol β and pol λ in this regard are currently under investigation. It is also possible that a short piece of terminal DNA downstream from the 1 nt gap opposite 8-oxo-dG is removed and a replicative, not a gap-filling, synthesis reinitiates opposite 8-oxo-dG.

ACKNOWLEDGEMENTS

We thank Luis Blanco, Carlos de los Santos, Paul Fisher, Fumio Hanaoka, Thomas Kunkel, Tomas Lindahl, Holly Miller, Haruo Ohmori, Larry Thompson, Alan Tomkinson and Roger Woodgate for enzymes and expression vectors. We also thank Cecilia Torres for oligonucleotide synthesis. This work was supported by NCI, National Institutes of Health, United States Public Health Service Grants (CA47995 and CA76163), the Ministry of Education, Culture, Sports, Science, and Technology of Japan (15025257), and the Japan Society for the Promotion of Science (15590347 and 16390119).

REFERENCES

1. Cooke,M.S., Evans,M.D., Dizdaroglu,M. and Lunec,J. (2003) Oxidative DNA damage: mechanism, mutation, and disease. *FASEB J.*, **17**, 1195–1214.
2. Shibutani,S., Takeshita,M. and Grollman,A.P. (1991) Insertion of specific bases during DNA synthesis past the oxidation-damaged base 8-oxodG. *Nature*, **349**, 431–434.
3. Wood,M.L., Dizdaroglu,M., Gajewski,E. and Essigmann,J.M. (1990) Mechanistic studies of ionizing radiation and oxidative mutagenesis: genetic effects of a single 8-hydroxyguanine (7-hydro-8-oxoguanine) residue inserted at a unique site in a viral genome. *Biochemistry*, **29**, 7024–7032.
4. Moriya,M. (1993) Single-stranded shuttle phagemid for mutagenesis studies in mammalian cells: 8-oxoguanine in DNA induces targeted G·C→T·A transversions in simian kidney cells. *Proc. Natl Acad. Sci. USA*, **90**, 1122–1126.
5. Parker,A.R. and Eshleman,J.R. (2003) Human MutY: gene structure, protein functions and interactions, and role in carcinogenesis. *Cell. Mol. Life Sci.*, **60**, 2064–2083.
6. Fortini,P., Pascucci,B., Parlanti,E., D'Errico,M., Simonelli,V. and Dogliotti,E. (2003) The base excision repair: mechanisms and its relevance for cancer susceptibility. *Biochimie*, **85**, 1053–1071.
7. Al-Tassan,N., Chmiel,N.H., Maynard,J., Fleming,N., Livingston,A.L., Williams,G.T., Hodges,A.K., Davies,D.R., David,S.S., Sampson,J.R. and Cheadle,J.P. (2002) Inherited variants of *MYH* associated with somatic G:C→T:A mutations in colorectal tumors. *Nature Genet.*, **30**, 227–232.
8. Xie,Y., Yang,H., Cunanan,C., Okamoto,K., Shibata,D., Pan,J., Barnes,D.E., Lindahl,T., McIlhatton,M., Fishel,R. and Miller,J.H. (2004) Deficiencies in mouse *myh* and *ogg1* result in tumor predisposition and G to T mutations in codon 12 of the *K-Ras* oncogene in lung tumors. *Cancer Res.*, **64**, 3096–3102.
9. Hirano,S., Tominaga,Y., Ichinoe,A., Ushijima,Y., Tsuchimoto,D., Honda-Ohnishi,Y., Ohtsubo,T., Sakumi,K. and Nakabeppu,Y. (2003) Mutator phenotype of MUTYH-null mouse embryonic stem cells. *J. Biol. Chem.*, **278**, 38121–38124.
10. Slupphaug,G., Kavli,B. and Krokan,H.E. (2003) The interacting pathways for prevention and repair of oxidative DNA damage. *Mutat. Res.*, **531**, 231–251.
11. Boldogh,I., Milligan,D., Lee,M.S., Bassett,H., Lloyd,R.S. and McCullough,A.K. (2001) hMYH cell cycle-dependent expression, subcellular localization and association with replication foci: evidence suggesting replication-coupled repair of adenine:8-oxoguanine mispairs. *Nucleic Acids Res.*, **29**, 2802–2809.
12. Parker,A., Gu,Y., Mahoney,W., Lee,S.H., Singh,K.K. and Lu,A-L. (2001) Human homolog of the MutY repair protein (hMYH) physically interacts with proteins involved in long patch DNA base excision repair. *J. Biol. Chem.*, **276**, 5547–5555.
13. Gu,Y., Parker,A., Wilson,T.M., Bai,H., Chang,D.-Y. and Lu,A-L. (2002) Human MutY homolog, a DNA glycosylase involved in base excision repair, physically and functionally interacts with mismatch repair proteins human MutS homolog 2/human MutS homolog 6. *J. Biol. Chem.*, **277**, 11135–11142.
14. Hayashi,H., Tominaga,Y., Hirano,S., McKenna,A.E., Nakabeppu,Y. and Matsumoto,Y. (2002) Replication-associated repair of adenine: 8-oxoguanine mispairs by MYH. *Curr. Biol.*, **12**, 335–339.
15. Parlanti,E., Fortini,P., Macpherson,P., Laval,J. and Dogliotti,E. (2002) Base excision repair of adenine/8-oxoguanine mispairs by an aphidicolin-sensitive DNA polymerase in human cell extracts. *Oncogene*, **21**, 5204–5212.
16. Fortini,P., Pascucci,B., Parlanti,E., D'Errico,M., Simonelli,V. and Dogliotti,E. (2003) 8-Oxoguanine DNA damage: at the crossroad of alternative repair pathways. *Mutat. Res.*, **531**, 127–139.
17. Caldecott,K.W., Tucker,J.D., Stanker,L.H. and Thompson,L.H. (1995) Characterization of the XRCC1-DNA ligase III complex *in vitro* and its absence from mutant hamster cells. *Nucleic Acids Res.*, **23**, 4836–4843.
18. Nash,R.A., Caldecott,K.W., Barnes,D.E. and Lindahl,T. (1997) XRCC1 protein interacts with one of two distinct forms of DNA ligase III. *Biochemistry*, **36**, 5207–5211.
19. Chou,K.M. and Cheng,Y.C. (2002) An exonucleolytic activity of human apurinic/apyrimidinic endonuclease on 3′ mispaired DNA. *Nature*, **415**, 655–659.
20. Mackey,Z.B., Ramos,W., Levin,D.S., Walter,C.A., McCarrey,J.R. and Tomkinson,A.E. (1997) An alternative splicing event which occurs in mouse pachytene spermatocytes generates a form of DNA ligase III with distinct biochemical properties that may function in meiotic recombination. *Mol. Cell. Biol.*, **17**, 989–998.
21. Bhagwat,A.S., Sanderson,R.J. and Lindahl,T. (1999) Delayed DNA joining at 3′ mismatches by human DNA ligases. *Nucleic Acids Res.*, **27**, 4028–4033.
22. Moriya,M. and Grollman,A.P. (1993) Mutations in the *MutY* gene of *Escherichia coli* enhance the frequency of targeted G:C→T:A transversions induced by a single 8-oxoguanine residue in single-stranded DNA. *Mol. Gen. Genet.*, **239**, 72–76.
23. Podlutsky,A.J., Dianova,I.I., Podust,V.N., Bohr,V.A. and Dianov,G.L. (2001) Human DNA polymerase β initiates DNA synthesis during long-patch repair of reduced AP sites in DNA. *EMBO J.*, **20**, 1477–1482.

24. Parlanti,E., Pascucci,B., Terrados,G., Blanco,L. and Dogliotti,E. (2004) Aphidicolin-resistant and -sensitive base excision repair in wild-type and DNA polymerase β-defective mouse cells. *DNA Repair*, **3**, 703–710.
25. Ramadan,K., Shevelev,I.V., Maga,G. and Hubscher,U. (2002) DNA polymerase λ from calf thymus preferentially replicates damaged DNA. *J. Biol. Chem.*, **277**, 18454–18458.
26. Shimazaki,N., Yoshida,K., Kobayashi,T., Toji,S., Tamai,K. and Koiwai,O. (2002) Over-expression of human DNA polymerase lambda in *E.coli* and characterization of the recombinant enzyme. *Genes Cells*, **7**, 639–651.
27. Garcia-Diaz,M., Bebenek,K., Kunkel,T.A. and Blanco,L. (2001) Identification of an intrinsic 5′-deoxyribose-5-phosphate lyase activity in human DNA polymerase λ. *J. Biol. Chem.*, **276**, 34659–34663.
28. Matsumoto,Y. and Kim,K. (1995) Excision of deoxyribose phosphate residues by DNA polymerase β during DNA repair. *Science*, **269**, 699–702.
29. Bebenek,K., Tissier,A., Frank,E.G., McDonald,J.P., Prasad,R., Wilson,S.H., Woodgate,R. and Kunkel,T.A. (2001) 5′-Deoxyribose phosphate lyase activity of human DNA polymerase ι *in vitro*. *Science*, **291**, 2156–2159.
30. Haracska,L., Prakash,L. and Prakash,S. (2003) A mechanism for the exclusion of low-fidelity human Y-family DNA polymerases from base excision repair. *Genes Dev.*, **17**, 2777–2785.
31. Einolf,H.J. and Guengerich,F.P. (2001) Fidelity of nucleotide insertion at 8-oxo-7, 8-dihydroguanine by mammalian DNA polymerase δ. Steady-state and pre-steady-state kinetic analysis. *J. Biol. Chem.*, **276**, 3764–3771.
32. Tominaga,Y., Ushijima,Y., Tsuchimoto,D., Mishima,M., Shirakawa,M., Hirano,S., Sakumi,K. and Nakabeppu,Y. (2004) MUTYH prevents OGG1 or APEX1 from inappropriately processing its substrate or reaction product with its C-terminal domain. *Nucleic Acids Res.*, **32**, 3198–3211.

Published online January 23, 2004

Nucleic Acids Research, 2004, Vol. 32, No. 2 477–487
DOI: 10.1093/nar/gkh214

Identification and characterization of two forms of mouse MUTYH proteins encoded by alternatively spliced transcripts

Akimasa Ichinoe[1,2], Mehrdad Behmanesh[1], Yohei Tominaga[1], Yasuhiro Ushijima[1], Seiki Hirano[1], Yasunari Sakai[1], Daisuke Tsuchimoto[1], Kunihiko Sakumi[1], Norio Wake[2] and Yusaku Nakabeppu[1,*]

[1]Division of Neurofunctional Genomics, Department of Immunobiology and Neuroscience, Medical Institute of Bioregulation, Kyushu University, and Core Research for Evolutional Science and Technology (CREST), Japan Science and Technology Agency (JST), Fukuoka 812–8582, Japan and [2]Division of Molecular and Cell Therapeutics, Department of Molecular Genetics, Medical Institute of Bioregulation, Kyushu University, Tsurumihara 4546, Beppu, Oita 874–0838, Japan

Received October 22, 2003; Revised December 8, 2003; Accepted December 16, 2003 DDBJ/EMBL/GenBank accession nos+

ABSTRACT

There are three types of mouse *Mutyh* mRNAs (type a, b and c) generated by alternative splicing, and type b mRNA is a major form among the three in most of the tissues examined. The level of type c mRNA is relatively high in brain. Type a and b mRNAs were expected to encode 57.7 kDa protein (MUTYHα), while type c mRNA had a partly different open reading frame encoding a 50.2 kDa protein (MUTYHβ). An *in vitro* translation of type b and c mRNAs produced a 50 kDa MUTYHα and 47 kDa MUTYHβ, respectively. MUTYHα and MUTYHβ were detected in wild-type embryonic stem (ES) cells or thymocytes prepared from wild-type mice, but neither MUTYH-null ES cells nor thymocytes prepared from MUTYH-null mice. Both MUTYHα and MUTYHβ were mainly localized in the nuclei and some in mitochondria in wild-type ES cells. Recombinant MUTYHα and β were expressed as fusion proteins with thioredoxin in *Escherichia coli*, but only MUTYHα was partly soluble and thus could be purified. Recombinant MUTYHα possessed DNA glycosylase activities to excise adenine opposite 8-oxoguanine and guanine but not AP lyase activity.

INTRODUCTION

Cellular DNA is at high risk of being oxidized by reactive oxygen species, which are inevitably generated by normal metabolic functions such as mitochondrial respiration or by environmental exposure to ionizing radiation and chemicals. The oxidation of DNA has been shown to apparently result in either spontaneous mutagenesis or cell death (1,2), thus causing various age-related diseases such as cancer and neurodegeneration (3,4). Among the various types of oxidized damage in DNA, 8-oxoguanine (8-oxoG), an oxidized form of guanine, can pair with adenine as well as cytosine during DNA replication, and this action is considered to be one of the spontaneous causes of a G:C to T:A transversion mutation (5).

To minimize such spontaneous mutagenesis, organisms come equipped with elaborated repair enzymes, namely 8-oxoG DNA glycosylase which excises 8-oxoG opposite cytosine in DNA, and adenine DNA glycosylase which removes adenine incorporated opposite 8-oxoG in template DNA (6). In *Escherichia coli*, *mutM* (*fpg*) gene encoding the former DNA glycosylase, and *mutY* gene encoding the latter play important roles in the prevention of such spontaneous mutagenesis, especially in G:C to T:A transversion mutation (7). Most eukaryotic cells also possess either a MutM homolog or its functional homolog, OGG1 for the repair of 8-oxoG, and a MutY homolog (MUTYH or MYH) for the repair of adenine opposite 8-oxoG (3,8).

Recently, familial alterations in the human *MUTYH* gene have been reported to be possible causative mutations for certain types of autosomal recessive colorectal adenomatous polyposis (9–12), thus suggesting that the absence of the MUTYH function in human cells might also result in a mutator phenotype. Among the many genes involved in base excision repair (BER), *MUTYH* is the first candidate gene for a hereditary neoplasm in human beings. We recently generated MUTYH-null mouse embryonic stem (ES) cell lines (2), and reported that the spontaneous mutation rate in the MUTYH-null cells increased 2-fold in comparison to wild-type cells, thus indicating that the absence of the MUTYH function in mammalian cells results in a moderate mutator phenotype.

In human cells, we previously reported that there are three major *MUTYH* transcripts, namely type α, β and γ with a different 5′ sequence or first exon and each transcript is alternatively spliced, thus multi-forms of human MUTYH

*To whom correspondence should be addressed. Tel: +81 92 642 6800; Fax: +81 92 642 6791; Email: yusaku@bioreg.kyushu-u.ac.jp

+AB117937–AB117939

(hMUTYH) proteins are present in the nuclei and in the mitochondria (13). hMUTYH protein encoded by type α mRNA possesses a mitochondrial targeting sequence (MTS), consisting of the amino terminal 14 residues which are required for its localization in the mitochondria (14), while those encoded by type β and γ mRNAs lack the MTS, and are localized in the nuclei. As a result, the subcellular localization of hMUTYH in human cells indicates that mitochondrial DNA is an important target for BER initiated by MUTYH as well as OGG1, probably because of their increased oxidative stress (15,16). Interestingly, rodent MUTYH proteins deduced from mouse and rat MUTYH cDNA clones lack an amino-terminal sequence corresponding to the MTS in hMUTYH (17), thus raising the question as to whether or not mitochondrial forms of MUTYH exist in rodents.

In the present study, we identified three alternatively spliced *Mutyh* mRNAs from mouse ES cells and mouse tissues, and found these *Mutyh* mRNAs to encode two different forms of mouse MUTYH (mMUTYH) protein. An analysis of the subcellular distribution of the two mMUTYH proteins revealed that these proteins are mostly localized in the nuclei and to some extent in the mitochondria.

MATERIALS AND METHODS

Oligonucleotides

Oligonucleotides shown in Table 1, were obtained from Greiner Japan, and Hokkaido System Science.

Isolation of genomic clones for *Mutyh*

Using the *Mutyh* type b cDNA as a probe, three independent phage clones were obtained from the λ phage genomic library for 129SvJ mouse (Stratagene).

RNA

Total RNA from the cultured cells and various tissues of C57BL6/J mice was prepared using ISOGEN (Nippon Gene), and total RNA from tissues of BALB/c mice were purchased from Clontech.

Quantitative RT–PCR

RT–PCR for *Mutyh* and *Gapdh* mRNA was performed as follows. First-strand cDNA, prepared using First-Strand cDNA Synthesis Kits (Amersham Biosciences) according to the manufacturer's instructions, was subjected to PCR. PCR was performed in 20 μl of a reaction mixture containing 10 mM Tris–HCl (pH 8.3), 50 mM KCl, 1.5 mM $MgCl_2$, 0.5 μl of the first-strand cDNA, 0.4 U of recombinant Taq DNA polymerase (Takara), 0.2 μM each primer, and 200 μM each deoxynucleoside triphosphate. The initial denaturation was performed at 94°C for 1 min and the amplification was performed by 27, 32, 37 and 40 cycles of denaturation at 94°C for 20 s, annealing at 55°C (mY5A2 + mY3TGA, *m*GA5 + mGA3), or at 58°C (mY5B1 + mY3A1), for 20 s and extension at 72°C for 35 s (mY5B1 + mY3A1), or for 60 s (mY5A2 + mY3TGA, mGA5 + mGA3), followed by additional extension at 72°C for 5 min. PCR products were subjected to agarose gel electrophoresis, and the band intensity on the gel stained with ethidium bromide was measured using LAS1000-plus Luminescent Image Analysis System (FUJIFILM).

Plasmids

Mutyh cDNAs (type b, c) obtained by RT–PCR of total RNA prepared from CCE28 ES cells using a primer set of mY5ATG + mY3TGA, were cloned into pT7BlueR (Novagen), generating pT7:mMUTYHα and pT7:mMUTYHβ, respectively. For the expression of two forms of mouse MUTYH protein in *E.coli*, type b and type c *Mutyh* cDNA were subcloned into pET32a(+) (Novagen), and resultant plasmids were designated as pET32a:mMUTYHα and pET32a:mMUTYHβ, and these plasmids encoded fusion proteins with thioredoxin (Trx-mMUTYHα, Trx-mMUTYHβ). For the stable expression of two forms of MUTYH protein in mouse ES cells, type b and type c *Mutyh* cDNA were subcloned into pcDNA3.1/Hygro(+) (Invitrogen). pcDEBΔ:EGFP and pcDEBΔ:EGFPm were previously described (18). A cDNA fragment with BamHI site (5′ end) and NotI site (3′ end) which encodes the MUTYHα was prepared by PCR using a primer set (mYe255-B1 + mY3B-N1) and pT7:mMUTYHα or pT7:mMUTYHβ as a template, and inserted into the HindIII–NotI site of pcDEBΔ:EGFPm to construct pcDEBΔ:mMUTYHα-EGFPm or pcDEBΔ:mMUTYHβ-EGFPm, respectively. A plasmid pcDEBΔ:COX8-EGFPm was prepared by inserting cDNA encoding the N-terminal 34 amino acid residues of cytochrome *c* oxidase subunit VIII into the HindIII–NotI site of pcDEBΔ:EGFPm (18). For the production of MUTYHβ specific antigen, a DNA fragment with NcoI site (5′ end) and BamHI site (3′ end) which encodes the unique N-terminal residues for MUTYHβ (1–64 aa) was prepared by PCR using a primer set (NSpE5-1 + BpE3-2) and pT7:mMUTYHβ as a template, and subcloned into NcoI–BamHI sites of pET8c-TrpE to generate pET8c:TrpE-mMUTYHβN which encodes TrpE-mMUTYHβN fusion protein, or into NcoI–BamHI sites of pET32a(+) to generate pET32a:mMUTYHβN which encodes Trx-mMUTYHβN fusion protein.

DNA sequencing

The nucleotide sequence was determined using either Dye Terminator or Dye Primer Cycle Sequencing FS Ready Reaction Kits and a model 377 automated DNA sequencer (Perkin Elmer), according to the manufacturer's instructions.

Antibodies against mMUTYHβN

Rabbit polyclonal antibodies against the fusion protein TrpE-mMUTYHβN were prepared as previously described (19). The antibodies were purified with the aid of antigen-affinity columns (Trx-mMUTYHβN-Sepharose column) (18,20). Briefly, antiserum against TrpE-mMUTYHβN was loaded onto the Trx-mMUTYHβN-Sepharose column, and the column was washed with Low E buffer [50 mM sodium phosphate buffer (pH 7.6), 0.1% Triton X-100] and 10 mM sodium phosphate buffer (pH 7.6). The bound antibodies were then eluted using buffer E [0.2 M glycine–HCl (pH 2.3), 0.1 M NaCl, 0.1% Triton X-100]. The eluted fraction was dialyzed against TBS [10 mM Tris–HCl (pH 7.5), 0.9% NaCl] and the purified antibodies were designated as anti-mMUTYHβN.

In vitro transcription and translation

Each type of *Mutyh* cDNA was placed under the control of the T7 promoter in pT7Blue vector (Novagen). The transcripts were synthesized from BamHI linearized plasmids by T7

Table 1. Oligonucleotides used in this study

Oligonucleotides	Sequences[a]
mY5B1	TCGGAGACTGCGCAGGAG
mY5ATG	ATTATCATGAAGAAACTCCAAGCAT
mY5A1	ATACTCGATGGATGCAGAAGT
mY5A2	CCTGGTGCAAAGGCCTGA
mY3TGA	GTATCACTGGGTAGTACTGTTG
mY3A1	GGGAAGCGCTGGCCAGGT
mY3A2	CCTCGAGAATAGTAGCCCAG
mYe255-β1	CGGGGATCCGATTATTATCATGAAGAAACTCCAAGCAT
mY3B-N1	TAAGCGGCCGCCTGGGTAGTACTGTTGGGTTTGT
YN13F	GTAAAACGACGGCCAGT
YNK	CGCTCTAGAACTAGTGGATC
mGA5-1	CTGCCATTTGCAGTGGCAAAG
mGA3-1	TGGTATTCAAGAGAGTAGGGA
NSpE5-1	TAACCATGGGTCGACAAATGGCCTGGCCAAGCAGAAGA
BpE3-2	ATTGGATCCTTACAGCATAGGCCCTCCTGTCC
*A	FAM-AGCGGCCATCGATACCGTCAACCTCGAGGAATTCC
GO	GGAATTCCTCGAGGTGOGACGGTATCGATGGCCGCT
G	GGAATTCCTCGAGGTGGACGGTATCGATGGCCGCT
19-P	FAM-AGCGGCCATCGATACCGTC-phosphate
19-OH	FAM-AGCGGCCATCGATACCGTC-OH

[a]FAM, 5′-end was labeled with FAM; GO, 8-oxoG; phosphate, 3′-end was attached to a phosphate group; OH, 3′-end was attached to a hydroxyl group; bold letter indicates a target base for nicking assay.

RNA polymerase at 30°C for 15 min using Single Tube Protein System 2 (Novagen). These mRNAs were translated in rabbit reticulocyte lysates in a total volume of 50 µl at 30°C for 60 min.

Cell culture

Wild-type mouse ES cell line, CCE28 and MUTYH-null ES cell line, YDK15, and COS-1 cells were maintained as previously described (2,21). For the expression of MUTYH protein in mouse ES cells, plasmid was electroporated into YDK15 cells, and stable transfectants grown in the presence of hygromycin B (140 and 160 µg/ml, Wako Pure Chemicals) were established. YDK15 cells expressing wild-type mMUTYHα was designated YDKα cells. YDK15 cells expressing a mutant mMUTYHβ was designated YDKβ.

Laser scanning fluorescence microscopy

COS-1 cells were cultured on slides and transfected with pcDEBΔ:EGFPm derivatives with the aid of LipofectAMINE (Invitrogen) according to the manufacturer's instructions. After 48 h of incubation at 37°C, cells were incubated with 2 µM MitoTracker Red CM-H2XROS (Molecular Probes) for 30 min, then the slides were observed under an Eclipse TE300 (Nikon) equipped with a Radiance 2100 laser scanning fluorescence microscope system (Bio-Rad).

Cell fractionation

The preparations of nuclear, cytosolic and mitochondrial fractions were all performed as previously described by Kang *et al.* (22).

Western blotting analysis

Protein samples were separated by SDS–PAGE, and then were transferred onto Immobilon-P membrane (Millipore), and western blotting analyses were performed as previously described (18), using anti-hMUTYH (13) and anti-mMUTYHβN.

Electron microscopic immunocytochemistry

Thin sections of fixed cells were prepared and processed for electron microscopic immunocytochemistry, as previously described (1,21).

Image processing

All digitized images were processed for publication using Adobe Photoshop 5.5J (Adobe Systems).

Statistical analysis

We performed the statistical analysis using StatView Version 5.0 (SAS Institute).

Purification of recombinant Trx-mMUTYH proteins

E.coli BL21(codonplus RIL) cells transformed with pET32a-mMUTYH were grown in LB medium (250 ml × 12 flasks), which was supplemented with ampicillin (50 µg/ml), 0.2 mM ammonium iron II and 0.2 mM ammonium sulfide, to an OD600 of 0.6–0.7 at 37°C with vigorous shaking. Protein expression was induced by addition of 0.4 mM isopropyl β-D-thiogalactoside (IPTG) to the cultures and incubation at 20°C for 10 h. The cells were washed, harvested and stored at –80°C. The cells (13 g wet weight from 3 liter culture) were suspended at room temperature for 30 min in 36 ml of buffer B containing 200 mM KCl, 5 mM β-mercaptoethanol and 20 mM HEPES–KOH (pH 7.8) with 0.1 mM PMSF, leupeptin (0.5 µg/ml), pepstatin (0.5 µg/ml), and chymostatin (0.5 µg/ml). The cells were disrupted by sonication and the cell lysates were clarified by centrifugation at 40 000 *g* for 30 min at 4°C. Two milliliters of 50% suspension of TALON Superflow metal affinity resin (Clontech) equilibrated with buffer B, was mixed with the cell lysate (FI, 20 ml) and gently rotated for 20 min at 4°C. Next, the resin was washed twice with 20 ml of buffer B containing 10 mM imidazole, and the resin was transferred into a column, washed with 10 ml of the same buffer. Elution was performed with buffer B containing 150 mM imidazole. Fractions (FII) containing Trx-MUTYH

protein were pooled and proteins were precipitated with 70% saturated ammonium sulfate. Precipitated proteins were resuspended in 100 µl of buffer B containing 500 mM KCl and 10% glycerol. The resuspended proteins were further separated through superose 12/30 (Amersham Biosciences) equilibrated with the same buffer, and 300 µl of fractions were collected. Fractions (FIII) containing a single band of Trx-MUTYH were stored at –80°C.

Determination of the protein concentration

The protein concentration was determined using a Bio-Rad protein assay kit (Bio-Rad) and BSA as the standard.

Nicking assay

Double-stranded oligonucleotide substrates summarized in Table 1 were prepared and then the standard nicking assay was performed, as previously described (2,13,15). Briefly, duplex oligonucleotides (20 nM) were incubated in 12.5 µl of a reaction mixture containing 10 mM Tris–HCl (pH 7.6), 5 µM $ZnCl_2$, 0.5 mM DTT, 0.5 mM EDTA, 1.5% glycerol, 100 µg/ml BSA and 40 nM Trx-mMUTYH at 37°C for 60 min. The reactions were heated in the presence of 0.67 N NaOH at 95°C for 5 min, and the products were extracted with phenol/chloroform, and precipitated with ethanol. Precipitated products were dissolved in 30 µl of 40% formamide containing 3 µg/ml BlueDextran (Sigma) and 10 mM EDTA, then 3 µl of the mixture was fractionated on 8% long Ranger denatured gel (24 cm length) containing 7 M urea at 30 W for 2 h.

RESULTS

Alternative splicing transcripts from *Mutyh* gene

To examine whether the mouse *Mutyh* gene encodes multiple transcripts as with the human *MUTYH* gene, we performed RT–PCR analysis of the total RNA prepared from mouse ES cells using two different sets of primers, mY5A1 + mY3TGA, and mY5ATG + mY3TGA, and an additional smaller cDNA was amplified with the latter set of primers, which cover the entire open reading frame of mMUTYH, in addition to the major 1.55 kb band which corresponds to the size expected from *Mutyh* cDNAs reported (Fig. 1A and B) (2). To obtain sequences for most 5′-regions of *Mutyh* mRNA, we next amplified *Mutyh* cDNA from mouse spleen cDNA library constructed in λZAPII vector, by nested PCR using two sets of primers (YN13F + mY3A2, YN7 + mY3A1), in which YN13F and YN7 hybridized to the multi-cloning site of the vector. Multiple bands were amplified and those were subcloned and sequenced (Fig. 1C). Sequence analysis revealed that there are three different *Mutyh* cDNAs (368, 440, 533 bp) corresponding to the bands shown with arrowheads in Figure 1C, with or without 93- and/or 74-base insertion, and that other smaller bands are incompletely elongated *Mutyh* cDNAs.

Based on the most 5′-sequence of the *Mutyh* cDNA obtained, we further performed a RT–PCR analysis of total RNA prepared from mouse ES cells and tissues of BALB/c mice using a primer set, mY5B1 + mY3A1. As shown in Figure 1D, three bands corresponding to 529, 436 and 362 bp fragments were detected, and thus transcripts corresponding to these cDNAs were designated as type a, b and c *Mutyh* mRNA, respectively. In each sample, type b mRNA was a major form of *Mutyh* mRNA and very low levels of type a and c mRNAs

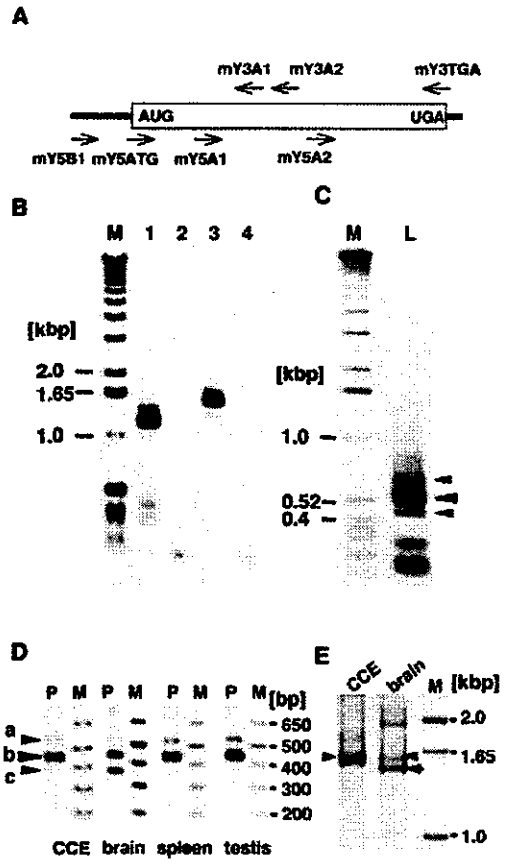

Figure 1. The detection of multiple forms of *Mutyh* mRNA in mouse embryonic stem cells and tissues. (A) Schematic diagram of *Mutyh* mRNA structure and primers used for the amplification of its cDNA. The primer sequences are listed in Table 1. (B) RT–PCR analysis of total RNA prepared from a mouse ES cell line, CCE28 cells. cDNA prepared from total RNA were amplified using two different sets of primers, mY5A1 + mY3TGA (lanes 1, 2), and mY5ATG + mY3TGA (lanes 3, 4). Template cDNA was omitted in the reactions for lanes 2 and 4. Lane M, markers. (C) Amplification of 5′-region of *Mutyh* cDNA. The mouse spleen cDNA library in λZAPII was initially amplified using a set of primers, YN13F + mY3A2, then a nested PCR was performed using a set of primers, YNK + mY3A1. YN13F and YNK hybridize to the multi-cloning site in the vector. Lane M, markers; lane L, PCR product. Three major PCR products are shown with arrowheads. (D) Detection of three types of *Mutyh* mRNA in ES cells and mouse tissues. cDNA prepared from total RNA extracted from CCE28 cells (CCE), brain, spleen and testis of BALB/c mice were amplified using a primer set of mY5B1 and mY3A1. The bands corresponding to types a, b and c are shown with arrowheads. Lane M, markers; lane P, PCR product. (E) Detection of full-length *Mutyh* mRNAs from mouse ES cells and tissue. cDNA prepared from total RNA prepared from CCE28 cells (CCE) and the brain were amplified using a set of primers, mY5B1 + mY3TGA, for 40 cycles. Lane M, markers. Arrowheads indicate 1.6 kb bands, and an arrow indicates the smaller cDNA amplified from brain RNA.

were detected, but in brain, type c was as abundant as type b. These cDNA fragments were again subcloned, and their sequences were confirmed (data not shown). To examine whether there were full-length mRNAs carrying these alternative 5′ sequences, we again performed RT–PCR analysis of total RNA prepared from CCE28 cells and brain using a primer set, mY5B1 + mY3TGA. A major 1.6 kb band corresponding to the full-length type b cDNA was amplified from CCE28 RNA, while a slightly smaller band corresponding to the full-length type c cDNA, as well as the 1.6 kb band

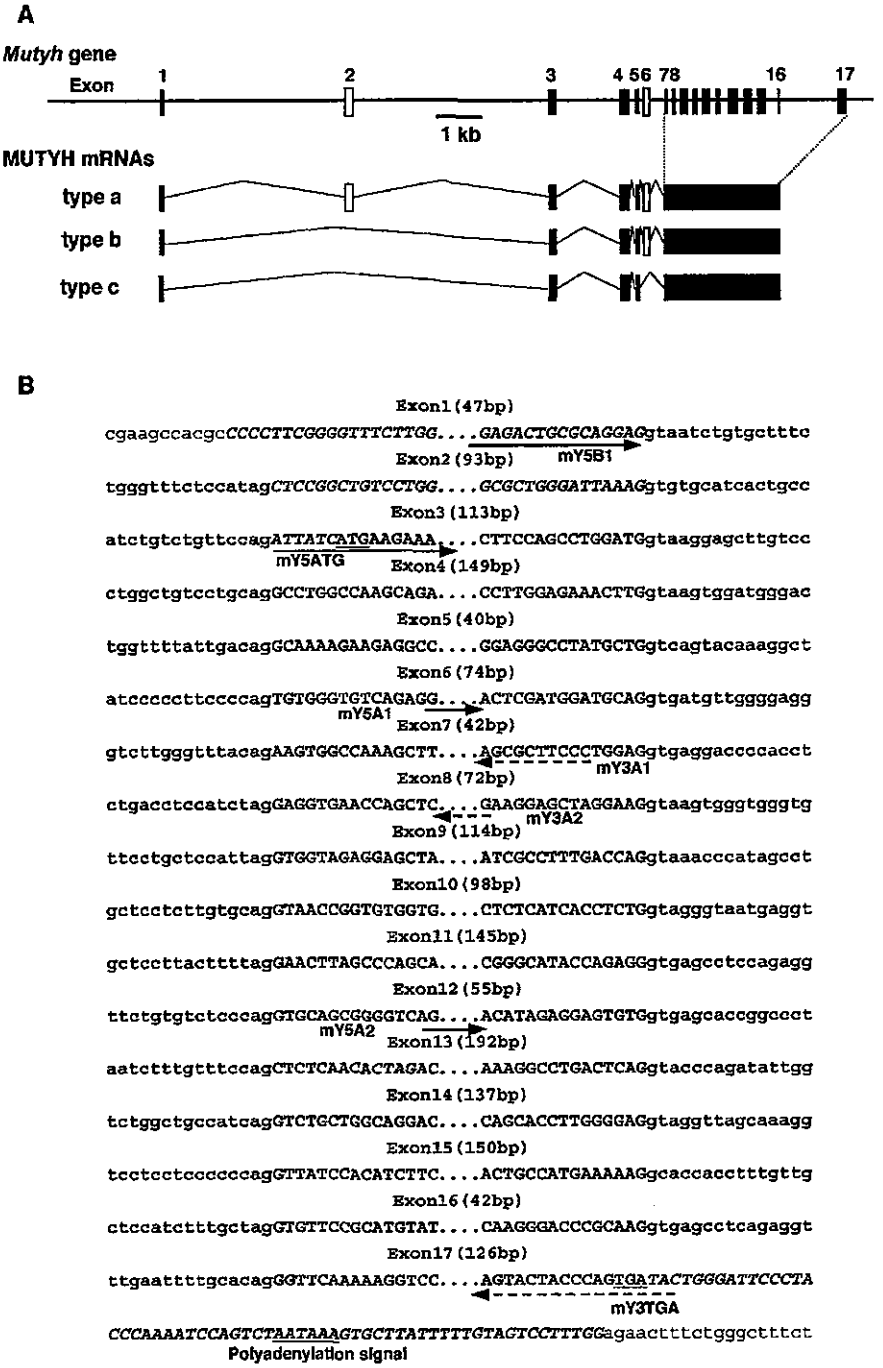

Figure 2. Genomic organization and alternative splicing of *Mutyh* gene. (**A**) Schematic diagram of the structure of *Mutyh* gene and its transcripts. The structure of the gene is shown in the upper part. Each exon is shown as a box, and alternative exons, 2 and 6 are shown in open boxes. Three types of alternatively spliced *Mutyh* mRNAs are shown. (**B**) The nucleotide sequences of intron/exon boundaries of *Mutyh* gene. The nucleotide sequences of exons and parts of introns determined by comparison of sequences of three types of *Mutyh* cDNAs [Y.Nakabeppu and A.Ichinoe (2003) DDBJ/EMBL/GenBank accession nos. AB117937, AB117938 and AB117939] with mouse genomic sequence [S.Blakey (2002) DDBJ/EMBL/GenBank accession no. AL683847], are shown in bold uppercase and lowercase, respectively, and the flanking sequences in plain lowercase. The genomic sequences shown were confirmed by the sequencing of phage clones from a λ phage genomic DNA library derived from 129SvJ mouse. The start of exon 1 was based on the longest EST clone for *Mutyh* mRNA [Y.Hayashizaki (2002) DDBJ/EMBL/GenBank accession no. BY181655]. The initiation codon ATG, the termination codon TGA and a putative polyadenylation signal are underlined. Positions of primers shown in Figure 1A are also shown with arrows: solid arrows, 5′-side primers; dotted arrows, 3′-side primers.

was amplified from brain RNA (Fig. 1E), thus confirming that there are at least two types of full-length *Mutyh* mRNAs in mouse brain.

Then we isolated several independent phage clones from a λ phage genomic DNA library derived from 129SvJ mouse, and determined sequences flanking each exon. The *Mutyh* gene

spans 12 kb and consists of 17 exons (Fig. 2B), and sequence comparison with the three types of *Mutyh* cDNA revealed that exon 2 and exon 6 are alternatively spliced to generate three types of *Mutyh* transcripts, namely type a, b and c (Fig. 2A). The sequence of each exon–intron junction was completely conserved in *Mutyh* gene of C57BL/6J strain [S.Blakey (2002) DDBJ/EMBL/GenBank accession no. AL683847].

To compare the expression level of each *Mutyh* transcript in various mouse tissue, quantitative RT–PCR for *Mutyh* and *Gapdh* mRNAs was performed using RNA prepared from C57BL/6J mouse tissues. The expression level of *Mutyh* mRNA was determined by amplifying the common 3′-region for the three types of *Mutyh* mRNA with a primer set of mY5A2 and mY3TGA, and was normalized to that of *Gapdh* mRNA (Fig. 3, top and middle panels). Thymus, small intestine, lung and heart expressed high levels of *Mutyh* mRNAs, and cerebellum, large intestine, liver and cerebrum expressed slightly lower levels of *Mutyh* mRNA than did the former. The expression level of *Mutyh* mRNA in thymus was the highest among all examined tissues.

In order to compare expression levels of the three types of *Mutyh* mRNAs in each tissue, RT–PCR with a primer set of mY5B1 + mY3A1 was performed (Fig. 3, bottom panel). In most tissues examined, type b mRNA was the major form, while in the cerebellum almost equal amounts of type b and c *Mutyh* mRNAs were detected. Relatively high levels of type c mRNA were detected in the cerebrum, heart, lung and thymus in addition to cerebellum, while much lower levels of type a *Mutyh* mRNA were detected in some tissues such as the large intestine. As a result, we concluded that three types of *Mutyh* mRNA formed by alternative splicing were indeed expressed *in vivo*, and their expression levels vary among tissues.

Two types of mouse MUTYH protein encoded by alternatively spliced transcripts

Among the three types of *Mutyh* mRNAs, type a and type b completely share their open reading frames, indicating that they encode the same mMUTYH protein, namely mMUTYHα (516 aa, MW: 57 686), while type c mRNA shares only the C-terminal part of its open reading frame with those of type a and b (Fig. 4A), and thus encoding mMUTYH protein with a unique N-terminus, designated as mMUTYHβ (429 aa, MW: 47 197) (Fig. 4B). As shown in Figure 5A, bands corresponding to 50–54 kDa, which reacted with anti-hMUTYH antibody, were produced by an *in vitro* translation of type b *Mutyh* mRNA, while 45–47 kDa bands were detected in an *in vitro* translation product of type c *Mutyh* mRNA by the anti-hMUTYH. mRNA for the nuclear type of hMUTYH produced a polypeptide which co-migrated with mMUTYHα.

By western blotting analysis using anti-hMUTYH (Fig. 5B), two upper bands whose sizes were approximately 50–54 kDa and one lower band corresponding to a 47 kDa polypeptide were detected in the wild-type ES cell line, CCE28 cells but not a MUTYH-null ES cell line, YDK15 cells. YDKα cells which received an expression vector for type b *Mutyh* cDNA restored expression of the upper bands but not the lower band, while YDKβ cells which received an expression vector for type c *Mutyh* cDNA restored only expression of the lower band, thus confirming that the two forms of mMUTYH protein encoded by alternatively spliced *Mutyh* mRNAs were indeed expressed in ES cells. The expression of the two forms of

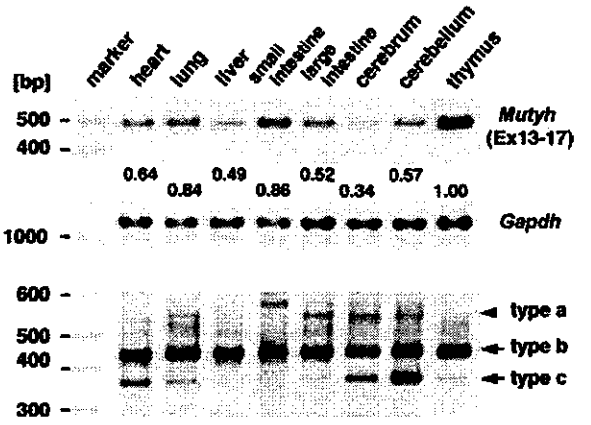

Figure 3. The expression of *Mutyh* mRNA in various mouse tissues. cDNAs were prepared from total RNA extracted from various mouse tissues, and the common 3′-region for the three types of *Mutyh* mRNA including exons 13–17 were amplified with a set of primers of mY5A2 + mY3TGA (top panel). The relative amount of total *Mutyh* mRNA in each tissue to that in thymus, which was normalized by the level of *Gapdh* mRNA (middle panel), is shown under each lane. Data from amplification for 32 cycles are shown, which achieved a linear range of amplification. The 5′-parts of three types of *Mutyh* cDNA (type a, b, c) were competitively amplified with a primer set of mY5B1 + mY3A1 for each tissue, and data from amplification for 40 cycles are shown (bottom panel).

mMUTYH protein was confirmed in thymocytes prepared from wild-type but not MUTYH-null mice (Fig. 5C), although in MUTYH-null thymocytes, there was a minor 50 kDa band reactive with anti-hMUTYH. We raised antibodies against the amino-terminal region of mMUTYHβ, namely anti-mMUTYHβN, and the anti-mMUTYHβN detected a 47 kDa band only in wild-type thymocytes, thus supporting the expression of mMUTYHβ in wild-type mice, as expected from the RT–PCR analysis findings shown in Figure 3.

Subcellular localization of two forms of mMUTYH protein in mouse ES cells

Whole cell extracts, nuclear, cytosolic and mitochondrial fractions were prepared from CCE28 and YDK15 cells, and subjected to western blot analysis using anti-hMUTYH. As shown in Figure 6, a few bands were detected in each fraction, and 50–54 kDa bands detected only in CCE28 cells were mostly recovered in the nuclear fraction, and some in the mitochondrial fraction. However, a faint 54 kDa band was also seen in YDK15 cells. It is thus likely that a mitochondrial mMUTYH, if any, comigrates with the nonspecific band detected in YDK15 cells. A 47 kDa mMUTYHβ, was hardly detected in any fraction, because its expression level was very low.

To further evaluate the subcellular localization of mMUTYH in mouse cells, we next prepared thin sections from fixed CCE28, YDK15, YDKα and YDKβ cells and the intracellular localization of the authentic mMUTYH was analyzed by electron microscopic immunocytochemistry, using anti-hMUTYH in combination with protein A-gold (Fig. 7A). In each of the nuclear and mitochondrial regions from CCE28 cells, specific signals were observed. However, no such signal was observed in YDK15 cells, thus confirming that mMUTYH is indeed localized in the mitochondria as well as in nuclei.

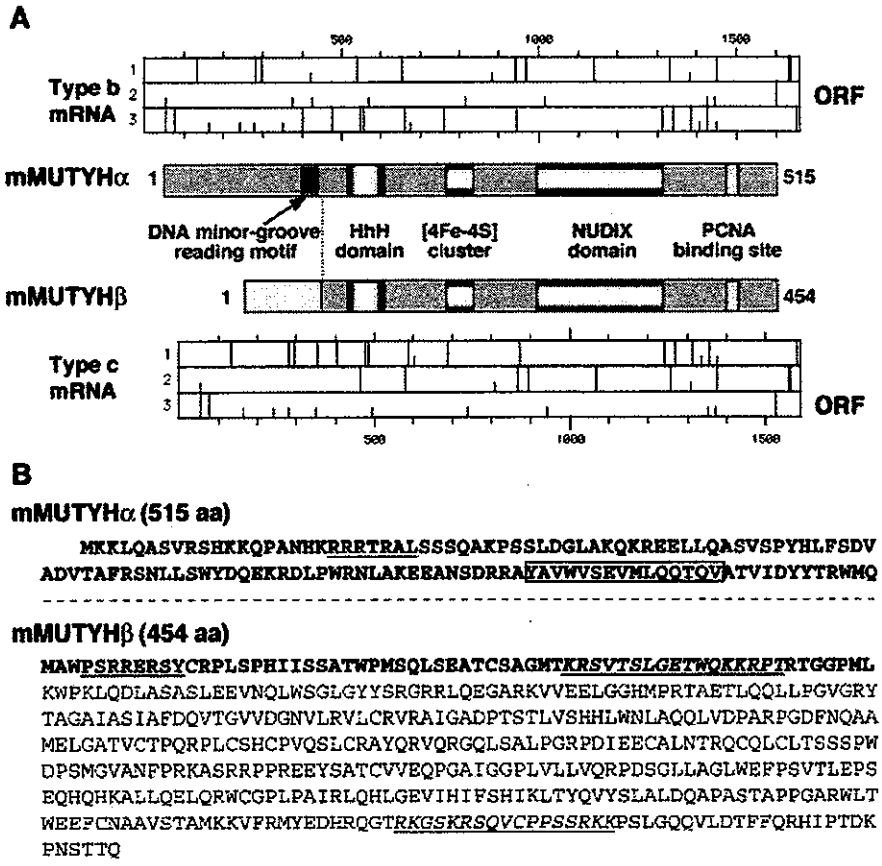

Figure 4. Alternatively spliced transcripts of the *Mutyh* gene encode two different forms of mMUTYH proteins. (**A**) Two forms of mMUTYH protein encoded by type b and c *Mutyh* mRNAs. The functional motifs in mMUTYHα encoded by type a and b mRNAs and mMUTYHβ encoded by type c mRNA are shown in the middle part. mMUTYHβ lacks the DNA minor groove reading motif (black box) present in mMUTYHα (25). An initiation codon (AUG, short bar) and stop codons (long bar) in each three reading frames (1, 2, 3) of type b and type c *Mutyh* mRNAs are shown in the upper (type b), and the lower part (type c). ORF, open reading frame for each mRNA. (**B**) The amino acid sequences of mMUTYHα and mMUTYHβ proteins. Differences in the amino acid sequences between the two MUTYH proteins are shown in bold. In MUTYHα, the common sequences with MUTYHβ are omitted (- - -). MTS-like sequences are underlined, while NLS-like sequences are shown in italic and are underlined. The boxed sequence in mMUTYHα indicates the DNA minor groove reading motif missing in mMUTYHβ.

In YDKα and YDKβ cells, slightly less signals were observed both in nuclei and mitochondria. We counted the number of signals in the nuclear and mitochondrial regions in each section (Fig. 7B), and the number of both nuclear and mitochondrial signals in CCE28, YDKα and YDKβ cells were significantly higher than those in YDK15 cells.

Recombinant mMUTYHα and mMUTYHβ fused to EGFP were expressed in COS-1 cells, and their fluorescence was mostly detected in the nuclei and to a lesser extent in the cytoplasm, and was partly merged with MitoTracker, a mitochondrial fluorescent marker (Fig. 8). EGFP itself was evenly distributed in COS-1 cells, while EGFP fused to COX8 mitochondrial targeting sequence was exclusively localized in mitochondria, thus indicating that mMUTYHα and mMUTYHβ are both mostly localized in the nuclei and to a much lesser extent in the mitochondria in mouse ES cells.

Mouse MUTYHα specifically excises adenine opposite 8-oxoguanine and guanine, but lacks AP lyase activity

In order to characterize the biochemical properties of mMUTYHα and mMUTYHβ, we expressed these proteins as thioredoxin fusion proteins (Trx-mMUTYHα, Trx-mMUTYHβ) in *E.coli*. As shown in Figure 9A, both fusion proteins were abundantly expressed, however only a part of Trx-mMUTYHα, but not Trx-mMUTYHβ, was able to be recovered in a soluble fraction. We purified Trx-mMUTYHα through two-step column chromatography to near homogeneity (Fig. 9B).

The activities introducing a single strand nick into substrates containing adenine opposite 8-oxoG, or adenine opposite guanine, were detected in the purified Trx-mMUTYHα preparation, only after NaOH treatment (Fig. 9C). The cleaved product after NaOH treatment comigrated with a marker oligonucleotide with the 3′-phosphate group (19-P) but not with the 3′-hydroxy group (19-OH), indicating that Trx-mMUTYHα does not possess AP-lyase activity at all.

DISCUSSION

Among three genes, *MTH1*, *OGG1* and *MUTYH* which play essential roles in preventing spontaneous mutagenesis due to

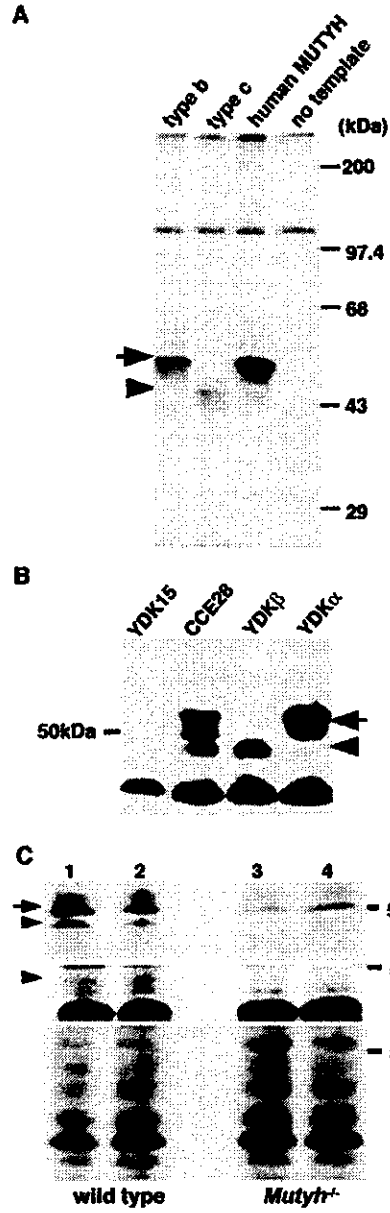

Figure 5. Two forms of mMUTYH protein encoded by the alternatively spliced transcripts. (A) *In vitro* translation of type b and type c *Mutyh* mRNAs. RNAs synthesized from pT7Blue plasmids carrying type b and type c *Mutyh* cDNA or human *MUTYH* cDNA for nuclear hMUTYH (13) by T7 RNA polymerase were translated using rabbit reticulocyte lysate, and translation products were subjected to a western blot analysis with anti-hMUTYH antibody. No template, during *in vitro* translation, template RNA was omitted. An arrow indicates 50 kDa mMUTYHα encoded by type b mRNA, and an arrowhead indicates the 47 kDa mMUTYHβ encoded by type c mRNA, respectively. (B) The detection of two forms of MUTYH in mouse ES cells. Whole cell extracts prepared from wild-type ES cell line, CCE28 cells, MUTYH-null YDK15 cells, and YDKα or YDKβ cells to which an expression construct for type b or type c cDNA was stably introduced, respectively, were subjected to western blot analysis with anti-hMUTYH antibody. An arrow indicates mMUTYHα and an arrowhead indicates mMUTYHβ, respectively. (C) The detection of two forms of mMUTYH protein in mouse thymocytes. Thymocyte extracts prepared from two independent wild-type (lanes 1, 2) and MUTYH-null mice (*Mutyh*$^{-/-}$; lanes 3, 4) were subjected to western blot analysis with anti-hMUTYH antibody (top panel), or with anti-mMUTYHβN (middle panel). An arrow indicates mMUTYHα and an arrowhead indicates mMUTYHβ, respectively. Stained filter with Coomassie Brilliant Blue is shown (*bottom*) for loading control.

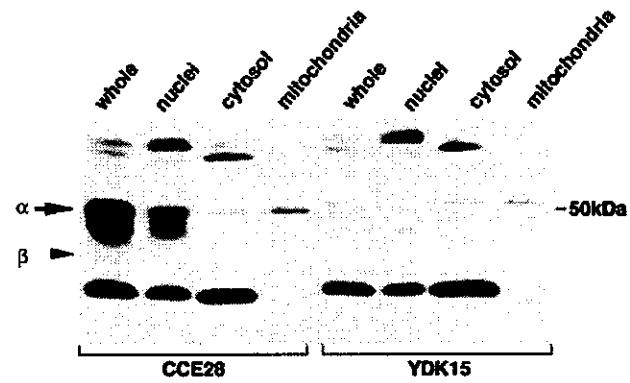

Figure 6. Subcellular localization of mMUTYH in mouse ES cells. Whole cell lysate (*whole*, 100 μg protein), nuclear fraction (nuclei, 100 μg protein), cytosolic fraction (cytosol, 25 μg protein) and mitochondrial fraction (mitochondria, 5 μg protein) prepared from wild-type CCE28 cells and MUTYH-null YDK15 cells were subjected to western blotting with anti-hMUTYH.

oxidative damage in nucleic acids, *MUTYH* gene has been widely noticed because of its alteration in patients with autosomal recessive colorectal adenomatous polyposis and colorectal cancer (9–12). We recently demonstrated that a disruption of *Mutyh* gene in mouse embryonic stem cells resulted in a mutator phenotype (2), and we have obtained data supporting the view that MUTYH-null mice are indeed predisposed to colorectal adenomatous polyposis and colorectal cancer (K.Sakamoto, Y.Tominaga, K.Yamauchi, Y.Nakatsu, K.Sakumi, K.Yoshiyama, A.Asaeda, A.Egashira, S.Kura, T.Yao, M.Tsuneyoshi, H.Maki, Y.Nakabeppu and T.Tsuzuki, manuscript in preparation). In the present study, we intensively characterized the expression of mouse *Mutyh* gene and its products both in embryonic stem cells and various mouse tissues, to gain an understanding of the physiological role of MUTYH protein *in vivo*.

The mouse *Mutyh* gene is located on chromosome 4, and consists of 17 exons among which exons 2 and 6 are alternatively spliced to generate three types of transcripts, type a, b and c. Type a and b transcripts of *Mutyh* produce 50 kDa polypeptide, namely mMUTYHα, while type c produces 47 kDa polypeptide, mMUTYHβ. In human cells, the *MUTYH* gene encodes more than 10 transcripts generated by alternative transcription initiation as well as alternative splicing, and those mRNAs produce more than seven different forms of hMUTYH proteins (13). We and others have demonstrated that hMUTYH polypeptide (522 aa) encoded by type β3, β5 or γ3 mRNAs are localized in the nucleus and other isoforms of hMUTYH (546 aa, 536 aa, 535 aa) encoded by type α1, α2 and α3 mRNA are localized in the mitochondria, and that the latter possess MTS at their amino terminal ends, while the former, which are translated from an initiation codon corresponding to the second AUG in the latter, lack MTS (13,14). There is a further amino-terminally truncated form of hMUTYH (429 aa) encoded by type α4 and type γ4 mRNAs in human cells (13). mMUTYHα corresponds to the nuclear form of hMUTYH, while mMUTYHβ corresponds to the last form of hMUTYH whose expression is also high in brain.

We demonstrated the expression of two forms of mMUTYH polypeptide in mouse ES cells and thymocytes as well as

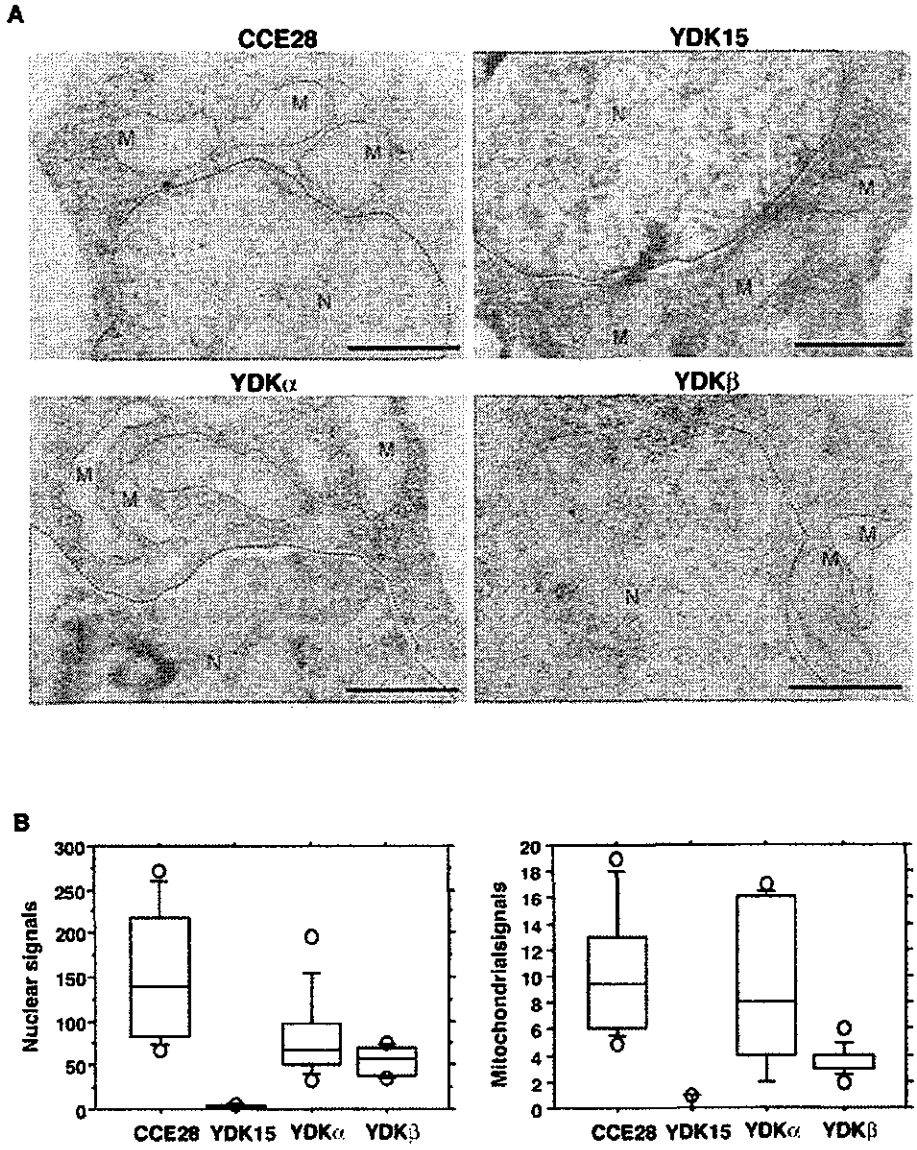

Figure 7. Intracellular localization of mMUTYH proteins. (A) Electron microscopic immunocytochemistry. Thin sections were prepared from fixed wild-type CCE28 cells, MUTYH-null YDK15 cells, mMUTYHα-expressing YDKα cells, and mMUTYHβ-expressing YDKβ cells. MUTYH signals were examined by electron microscopic immunocytochemistry, using anti-hMUTYH. Nuclear and mitochondrial structures are shown with blue and red dotted lines, respectively. Bars: 1 μm. (**B**) The distribution of MUTYH signals in nuclear and mitochondrial region determined by electron microscopic immunocytochemistry. Gold signals present in nuclear and mitochondrial regions as seen in (A), from 10 sections of each sample were counted, and the number of signals in nuclear or mitochondrial region per section is shown in a box-and-whisker-plot. Each plot shows a box with ends at quartiles, and the statistical median as a horizontal line in the box. The whiskers extend to the farthest points that are not outliers (circles). Both in nuclei and mitochondria, the number of gold signals detected in CCE28, YDKα and YDKβ cells were significantly higher than those in YDK cells (Mann–Whitney *U*-test, $P \leq 0.0002$).

expression of three forms of *Mutyh* mRNA in various mouse tissues. The expression levels of *Mutyh* mRNAs are highest in the thymus, small intestine and lung among the tissues examined, and in any tissue, type b mRNA encoding mMUTYHα is a major form, while type a also encoding mMUTYHα is a minor form. The expression levels of type c mRNA encoding mMUTYHβ are highest in the cerebellum, cerebrum, heart and lung, thus suggesting that the efficiency of alternative splicing to produce each transcript varies among those tissues.

In ES cells and thymocytes, mMUTYHα is more abundant than mMUTYHβ, and both forms are mostly localized in the nuclei, and to some extent in the mitochondria in ES cells. Initially, we could not deduce any MTS-like sequence in either mMUTYHα or mMUTYHβ, however, we now suggest that both forms of mMUTYH protein possess different MTS-like sequences as shown in Figure 4B, which were predicted using the iPSORT prediction system (http://hypothesiscreator.net/iPSORT). In addition, it was predicted that both forms share a typical bipartite nuclear localization signal (NLS) in the

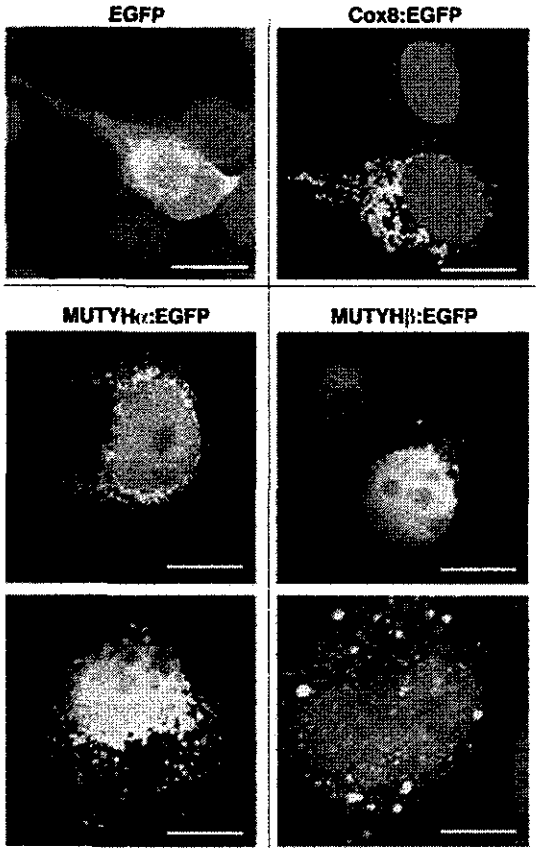

Figure 8. Expression of *Mutyh* cDNA in COS-1 cells. COS-1 cells transfected with plasmids encoding EGFP, COX8:EGFP, mMUTYHα:EGFP and mMUTYHβ:EGFP were incubated with MitoTracker (red) and fixed, then nuclei were stained with DAPI (blue). Cells were subjected to laser-scanning fluorescence microscopy. EGFP signals are shown in green and merged signals with MitoTracker (red) are seen in yellow. Bars: 20 μm.

common C-terminal region while mMUTYHβ possesses an additional bipartite NLS in its unique N-terminal region, by PSORT II server (http://psort.nibb.ac.jp) (Fig. 4B). Probably because of these NLSs, the majority of both forms of mMUTYH seem to be localized in the nuclei. Since oxidative stress is likely to be very high in the mitochondria, and thus the level of 8-oxoG in mitochondrial DNA is known to be higher than that in nuclear DNA (23), mitochondria come equipped with defense enzymes such as OGG1, MUTYH and MTH1 which play essential roles in avoiding errors caused by 8-oxoG (16). Human cell is equipped with hOGG1-2a which is exclusively located in mitochondria (15), however, only one form of OGG1 in rodent cell is likely to be located both in mitochondria as well as nuclei (8). Our results indicate that MUTYH protein also behaves similarly in rodent cells, suggesting that rodent cells may have a different sorting mechanism(s) for such repair proteins between nuclei and mitochondria. Nevertheless, our data indicate that MUTYH plays an important role in maintaining the genetic information in the mitochondrial genome as well as in the nuclear genome in mammalian cells.

To investigate the biochemical function of the two forms of mMUTYH protein, we prepared their recombinant form; however, we could only obtain mMUTYHα as a soluble form.

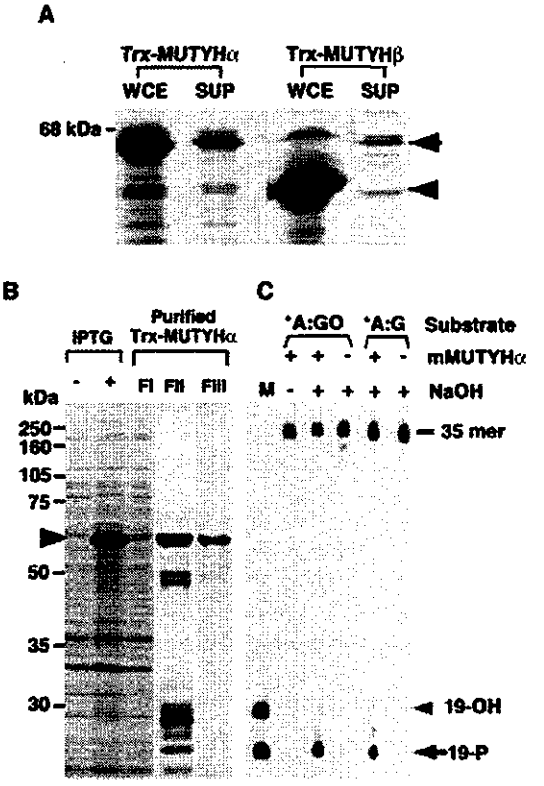

Figure 9. Expression and purification of recombinant mMUYTH proteins. (A) The expression of recombinant mMUTYH proteins. *E.coli* cells transformed with pET32a-mMUTYHα and pET32a-mMUTYHβ were grown in the presence of IPTG, and harvested cells were disrupted with sonication as described in Materials and Methods. Whole cell extracts (WCE) or supernatant after centrifugation (SUP) were subjected to western blotting with anti-hMUTYH. (B) Purification of recombinant Trx-mMUTYHα. *E.coli* cells transformed with pET32a-mMUTYHα were grown in the presence (+) or absence (–) of IPTG, and supernatant fraction (FI) was prepared from the harvested cells. Trx-mMUTYHα protein was purified using cobalt beads (FII) followed by gel filtration (FIII), as described in Materials and Methods. Each fraction was analyzed by SDS–PAGE and the gel was stained with Coomassie Brilliant Blue. (C) Biochemical characterization of purified Trx-mMUTYHα. Duplex oligonucleotide substrates containing A:8-oxoG (*A:GO) and adenine:guanine (*A:G) pairs, in which the 5′-end of one strand carrying target base adenine (*A) was labeled with FAM, were incubated with (+) or without (–) the purified Trx-mMUTYHα protein (FIII), as described in Materials and Methods, and the reaction products were fractionated by gel electrophoresis with (+) or without (–) NaOH treatment. M, marker oligonucleotides whose 5′-end was labeled with FAM (19-OH and 19-P).

Using recombinant protein, we demonstrated that mMUTYHα efficiently excises adenine opposite 8-oxoG and guanine as expected, but it lacks AP lyase activity. In the present study, we could not show any biochemical activity of mMUTYHβ, because of its unavailability *in vitro*. We expected that mMUTYHβ expressed in mouse ES cells may be available for such an *in vitro* study: however, it was somehow hard to establish cell lines expressing a large amount of mMUTYHβ in comparison to mMUTYHα. As a result, other expression systems should be examined for this purpose. It is noteworthy that the expression level of type c mRNA in brain or especially cerebellum is higher than in other tissues, thus suggesting that mMUTYHβ has a tissue-specific function. It was recently reported that hypoxia induces expression

of MUTYH in rat brain, and further that there are at least two isoforms of rat MUTYH (57, 50 kDa) and the 50 kDa isoform is abundant in neuronal mitochondria in the cerebrum and cerebellum (17,24).

It is very likely that the 50 kDa isoform of rat MUTYH corresponds to mMUTYHβ thus suggesting that mMUTYHβ or its equivalents in human and rat may have some function to protect the brain or neurons from DNA damage in mitochondria caused by hypoxia. Judging by their amino acid sequence (Fig. 4), such MUTYH isoforms may retain their binding activity to their substrate; however, it still remains to be clarified as to whether or not they retain DNA glycosylase activity, because they all lack the DNA minor groove reading motif (25).

It has now been established that patients with MUTYH mutations in both alleles are highly predisposed to tumorigenesis in the colon, and our long-term observation of MUTYH-null mice is likely to support this observation. In mice, the highest expression level of type b *Mutyh* mRNA was observed in the small intestine and to a lesser extent in the large intestine, where no type c mRNA was detected, thus suggesting that MUTYHα may be sufficient to prevent the occurrence of mutations in these tissues.

ACKNOWLEDGEMENTS

We thank Dr Masato Furuichi for helpful discussions, Akemi Matsuyama and Masafumi Sasaki for technical assistance, and Dr B. Quinn for comments on the manuscript. This work was supported by grants from the Ministry of Education, Culture, Sports, Science, and Technology of Japan (grant numbers: 15025257, 10480218, 1169420).

REFERENCES

1. Yoshimura,D., Sakumi,K., Ohno,M., Sakai,Y., Furuichi,M., Iwai,S. and Nakabeppu,Y. (2003) An oxidized purine nucleoside triphosphatase, MTH1 suppresses cell death caused by oxidative stress. *J. Biol. Chem.*, **278**, 37965–37973.
2. Hirano,S., Tominaga,Y., Ichinoe,A., Ushijima,Y., Tsuchimoto,D., Honda-Ohnishi,Y., Ohtsubo,T., Sakumi,K. and Nakabeppu,Y. (2003) Mutator phenotype of MUTYH-null mouse embryonic stem cells. *J. Biol. Chem.*, **278**, 38121–38124.
3. Nakabeppu,Y., Tominaga,Y., Tsuchimoto,D., Ide,Y., Hirano,S., Sakai,Y., Sakumi,K. and Furuichi,M. (2001) Mechanisms protecting genomic integrity from damage caused by reactive oxygen species: implications for carcinogenesis and neurodegeneration. *Environ. Mutagen. Res.*, **23**, 197–209.
4. Sakumi,K., Tominaga,Y., Furuichi,M., Xu,P., Tsuzuki,T., Sekiguchi,M. and Nakabeppu,Y. (2003) Ogg1 knockout-associated lung tumorigenesis and its suppression by Mth1 gene disruption. *Cancer Res.*, **63**, 902–905.
5. Shibutani,S., Takeshita,M. and Grollman,A.P. (1991) Insertion of specific bases during DNA synthesis past the oxidation-damaged base 8-oxodG. *Nature*, **349**, 431–434.
6. Michaels,M.L., Cruz,C., Grollman,A.P. and Miller,J.H. (1992) Evidence that MutY and MutM combine to prevent mutations by an oxidatively damaged form of guanine in DNA. *Proc. Natl Acad. Sci. USA*, **89**, 7022–7025.
7. Tajiri,T., Maki,H. and Sekiguchi,M. (1995) Functional cooperation of MutT, MutM and MutY proteins in preventing mutations caused by spontaneous oxidation of guanine nucleotide in *Escherichia coli*. *Mutat. Res.*, **336**, 257–267.
8. Boiteux,S. and Radicella,J.P. (1999) Base excision repair of 8-hydroxyguanine protects DNA from endogenous oxidative stress. *Biochimie*, **81**, 59–67.
9. Al-Tassan,N., Chmiel,N.H., Maynard,J., Fleming,N., Livingston,A.L., Williams,G.T., Hodges,A.K., Davies,D.R., David,S.S., Sampson,J.R. *et al.* (2002) Inherited variants of MYH associated with somatic G:C→T:A mutations in colorectal tumors. *Nature Genet.*, **30**, 227–232.
10. Jones,S., Emmerson,P., Maynard,J., Best,J.M., Jordan,S., Williams,G.T., Sampson,J.R. and Cheadle,J.P. (2002) Biallelic germline mutations in MYH predispose to multiple colorectal adenoma and somatic G:C→T:A mutations. *Hum. Mol. Genet.*, **11**, 2961–2967.
11. Sieber,O.M., Lipton,L., Crabtree,M., Heinimann,K., Fidalgo,P., Phillips,R.K., Bisgaard,M.L., Orntoft,T.F., Aaltonen,L.A., Hodgson,S.V. *et al.* (2003) Multiple colorectal adenomas, classic adenomatous polyposis and germ-line mutations in MYH. *N. Engl. J. Med.*, **348**, 791–799.
12. Sampson,J.R., Dolwani,S., Jones,S., Eccles,D., Ellis,A., Evans,D.G., Frayling,I., Jordan,S., Maher,E.R., Mak,T. *et al.* (2003) Autosomal recessive colorectal adenomatous polyposis due to inherited mutations of MYH. *Lancet*, **362**, 39–41.
13. Ohtsubo,T., Nishioka,K., Imaiso,Y., Iwai,S., Shimokawa,H., Oda,H., Fujiwara,T. and Nakabeppu,Y. (2000) Identification of human MutY homolog (hMYH) as a repair enzyme for 2-hydroxyadenine in DNA and detection of multiple forms of hMYH located in nuclei and mitochondria. *Nucleic Acids Res.*, **28**, 1355–1364.
14. Takao,M., Zhang,Q.M., Yonei,S. and Yasui,A. (1999) Differential subcellular localization of human MutY homolog (hMYH) and the functional activity of adenine:8-oxoguanine DNA glycosylase. *Nucleic Acids Res.*, **27**, 3638–3644.
15. Nishioka,K., Ohtsubo,T., Oda,H., Fujiwara,T., Kang,D., Sugimachi,K. and Nakabeppu,Y. (1999) Expression and differential intracellular localization of two major forms of human 8-oxoguanine DNA glycosylase encoded by alternatively spliced OGG1 mRNAs. *Mol. Biol. Cell*, **10**, 1637–1652.
16. Nakabeppu,Y. (2001) Regulation of intracellular localization of human MTH1, OGG1 and MYH proteins for repair of oxidative DNA damage. *Prog. Nucleic Acid Res. Mol. Biol.*, **68**, 75–94.
17. Englander,E.W., Hu,Z., Sharma,A., Lee,H.M., Wu,Z.H. and Greeley,G.H. (2002) Rat MYH, a glycosylase for repair of oxidatively damaged DNA, has brain-specific isoforms that localize to neuronal mitochondria. *J. Neurochem.*, **83**, 1471–1480.
18. Tsuchimoto,D., Sakai,Y., Sakumi,K., Nishioka,K., Sasaki,M., Fujiwara,T. and Nakabeppu,Y. (2001) Human APE2 protein is mostly localized in the nuclei and to some extent in the mitochondria, while nuclear APE2 is partly associated with proliferating cell nuclear antigen. *Nucleic Acids Res.*, **29**, 2349–2360.
19. Nakabeppu,Y. and Nathans,D. (1991) A naturally occurring truncated form of FosB that inhibits Fos/Jun transcriptional activity. *Cell*, **64**, 751–759.
20. Nakabeppu,Y., Oda,S. and Sekiguchi,M. (1993) Proliferative activation of quiescent Rat-1A cells by delta FosB. *Mol. Cell. Biol.*, **13**, 4157–4166.
21. Ide,Y., Tsuchimoto,D., Tominaga,Y., Iwamoto,Y. and Nakabeppu,Y. (2003) Characterization of the genomic structure and expression of the mouse *Apex2* gene. *Genomics*, **81**, 47–57.
22. Kang,D., Nishida,J., Iyama,A., Nakabeppu,Y., Furuichi,M., Fujiwara,T., Sekiguchi,M. and Takeshige,K. (1995) Intracellular localization of 8-oxo-dGTPase in human cells, with special reference to the role of the enzyme in mitochondria. *J. Biol. Chem.*, **270**, 14659–14665.
23. Ames,B., Shigenaga,M. and Hagen,T. (1993) Oxidants, antioxidants and the degenerative diseases of aging. *Proc. Natl Acad. Sci. USA*, **90**, 7915–7922.
24. Lee,H.M., Wang,C., Hu,Z., Greeley,G.H., Makalowski,W., Hellmich,H.L. and Englander,E.W. (2002) Hypoxia induces mitochondrial DNA damage and stimulates expression of a DNA repair enzyme, the *Escherichia coli* MutY DNA glycosylase homolog (MYH), *in vivo*, in the rat brain. *J. Neurochem.*, **80**, 928–937.
25. Guan,Y., Manuel,R.C., Arvai,A.S., Parikh,S.S., Mol,C.D., Miller,J.H., Lloyd,S. and Tainer,J.A. (1998) MutY catalytic core, mutant and bound adenine structures define specificity for DNA repair enzyme superfamily. *Nat. Struct. Biol.*, **5**, 1058–1064.

Growth retardation and dyslymphopoiesis accompanied by G_2/M arrest in APEX2-null mice

Yasuhito Ide, Daisuke Tsuchimoto, Yohei Tominaga, Manabu Nakashima, Takeshi Watanabe, Kunihiko Sakumi, Mizuki Ohno, and Yusaku Nakabeppu

APEX2/APE2 is a secondary mammalian apurinic/apyrimidinic endonuclease that associates with proliferating cell nuclear antigen (PCNA), and the progression of S phase of the cell cycle is accompanied by its expression. To determine the biologic significance of APEX2, we established APEX2-null mice. These mice were about 80% the size of their wild-type littermates and exhibited a moderate dyshematopoiesis and a relatively severe defect in lymphopoiesis. A significant accumulation of both thymocytes and mitogen-stimulated splenocytes in G_2/M phase was seen in APEX2-null mice compared with the wild type, indicating that APEX2 is required for proper cell cycle progression of proliferating lymphocytes. Although APEX2-null mice exhibited an attenuated immune response against ovalbumin in comparison with wild-type mice, they produced both antiovalbumin immunoglobulin M (IgM) and IgG, indicating that class switch recombination can occur even in the absence of APEX2. (Blood. 2004;104: 4097-4103)

Introduction

Oxidation or other chemical modification of nucleotides and genomic DNA is a major threat to living organisms because the damage inflicted may cause alterations in base pairs or may block progression of DNA replication and transcription. Base excision repair (BER) is one of the major cellular defense mechanisms for eliminating damaged bases in genomic DNA.[1,2] DNA glycosylases catalyze the first step of BER by excising the damaged bases, and leave apurinic/apyrimidinic (AP) sites. Among the various mammalian DNA glycosylases, uracil DNA glycosylase (UNG) and MutY homolog (MUTYH) excise misincorporated bases during DNA replication, and both enzymes associate with proliferating cell nuclear antigen (PCNA), a scaffold protein for DNA replication machinery[3,4]; thus, both can initiate replication-associated BER.[4-7] APEX2/APE2,[8,9] a secondary mammalian AP endonuclease, is known to associate with PCNA through its PCNA-binding motif whereas the major AP endonuclease, APEX1/APE1/HAP1/REF1,[7,10-12] does not possess PCNA-binding motif. Therefore, we hypothesize that APEX2 is responsible for the incision of AP sites in replication-associated BER.[8,9] APEX1 was reported to be essential for early embryonic development in mice.[13] However, it has not yet been established that AP endonuclease activity is essential for mammals because, in addition to DNA repair, APEX1 also functions as a redox regulator of transcription factors.[12] Investigating the functions of both APEX1 and APEX2 is considered to be essential to clarify the biologic importance of AP endonuclease activities. To explore the biologic significance of APEX2 in vivo, we established APEX2-null mice.[14] We report herein that APEX2-null mice exhibit growth retardation and dyshematopoiesis accompanied by G_2/M arrest.

Materials and methods

Cell culture

Isolated mouse splenocytes were cultured in RPMI 1640 medium (Invitrogen, Carlsbad, CA) supplemented with 10% fetal bovine serum (Invitrogen), 50 μM 2-mercaptoethanol, 100 U/mL streptomycin, and 100 U/mL penicillin at 37°C in a humidified chamber with 5% CO_2. APEX2-null mouse embryo fibroblasts (MEFs) were isolated from embryos (13.5 days postcoital), and were cultured in Dulbecco modified Eagle medium supplemented with 10% heat-inactivated fetal calf serum, 100 U/mL streptomycin, and 100 U/mL penicillin at 37°C in a humidified chamber with 5% CO_2. The cells were routinely maintained by a standard 3T3 protocol, and spontaneously immortalized cell lines were thus established.

APEX2 expression plasmids

Two expression vectors for recombinant APEX2, pcDNA3.1/Hygro(+): mAPEX2 and pIRES1hyg:mAPEX2, were constructed by inserting DNA fragments encoding mouse APEX2 into the multiple cloning sites of pcDNA3.1/Hygro(+) (Invitrogen) and pIRES1hyg (Clontech, Palo Alto, CA), respectively.

From the Division of Neurofunctional Genomics, Department of Immunobiology and Neuroscience, Medical Institute of Bioregulation; the Department of Orthopedic Surgery, Graduate School of Medicine; and the Division of Molecular Immunology, Research Center for Prevention of Infectious Diseases, Medical Institute of Bioregulation, Kyushu University, Fukuoka, Japan.

Submitted April 19, 2004; accepted August 2, 2004. Prepublished online as *Blood* First Edition Paper, August 19, 2004; DOI 10.1182/blood-2004-04-1476.

Supported by grants from CREST, Japan Science and Technology Agency, the Ministry of Education, Culture, Sports, Science, and Technology of Japan (no. 15025257) and the Japan Society for the Promotion of Science (nos. 15590347 and 16390119).

Y.I. and D.T. contributed equally to this study.

Reprints: Daisuke Tsuchimoto, Division of Neurofunctional Genomics, Medical Institute of Bioregulation, Kyushu University, 3-1-1 Maidashi, Higashi-ku, Fukuoka 812 8582, Japan; e-mail: daisuke@bioreg.kyushu-u.ac.jp.

The publication costs of this article were defrayed in part by page charge payment. Therefore, and solely to indicate this fact, this article is hereby marked "advertisement" in accordance with 18 U.S.C. section 1734.

Establishment of APEX2-null mice

Apex2-disrupted mice were established as described previously.[14] Genotypes were analyzed by Southern blotting or by polymerase chain reaction (PCR) with the use of mouse tail DNA. PCR primers used to detect the wild-type allele were as follows: U796M, 5′GCAAGGCATCTCAACTATGGCTC3′; and L1321, 5′CTTCTCATCTTTGGACTCTGG3′. Mp2-5, 5′CTACGCATCGGTAATGAAGG3′, and L1321 were used to detect mutated allele. All primers were purchased from Hokkaido System Science (Sapporo, Japan). APEX2 protein was detected by Western blotting with the use of a specific antibody as described under "Western blotting." Heterozygous female ($Apex2^{+/-}$) mice were backcrossed with C57BL/6J males ($Apex2^{+/Y}$). F_9 or F_{10} male mice were used in most experiments unless stated otherwise in the text. APEX2-null female mice were obtained among offspring of *Apex2* knock-out (KO) male mice and $Apex2^{+/-}$ female mice. All mice were maintained in an air-conditioned, light time-controlled, specific-pathogen–free room. The handling and killing of the animals were in accordance with the national prescribed guidelines, and ethical approval for the studies was granted by the Animal Experiment Committee of Kyushu University (Fukuoka, Japan).

Western blotting of APEX2

Cells were suspended in extract buffer (125 mM Tris-HCl [tris(hydroxymethyl)aminomethane–HCl], pH 6.8; 2% sodium dodecyl sulfate [SDS]; 5% glycerol) and disrupted by sonication. Cell lysates were then centrifuged at 100 000*g*. Protein concentrations of supernatant were analyzed by means of a DC Protein Assay Kit (Bio-Rad Laboratories, Mississauga, ON, Canada), and 25 μg protein per lane was subjected to SDS–polyacrylamide gel electrophoresis (SDS-PAGE) and Western blotting analysis with the use of anti-mAPEX2.

Body and organ weight analysis

All mice were measured for body weight 10 times simultaneously without anesthesia, and the mean value was calculated. To measure organ weights, mice were dissected under pentobarbital anesthesia (75 mg/kg), and abdominal vessels were cut for blood drainage. Each organ was carefully removed and immediately measured.

Thymocytes, splenocytes, and bone marrow cells

Thymus and spleen were ground with glass slides, and cells were suspended in ice-cold phosphate-buffered saline (PBS) or culture medium. Bone marrow cells were suspended in ice-cold PBS by means of a syringe with a needle. An aliquot of cell suspension was diluted, and cells were counted under a microscope. The remaining cells were subjected to other analyses.

Cell cycle analysis

Flow cytometric analysis of the cell cycle was performed as previously described.[15] The cells were prepared by Nonidet P40 (NP40) treatment for the naked nuclei preparation. Then, 1×10^6 cells were centrifuged, washed with PBS, and suspended in fluorescence-activated cell sorter (FACS) buffer containing 3.4 mM sodium citrate, 10 mM NaCl, 0.1% NP40, and 50 μg/mL propidium iodide for 1 hour at 4 °C The data were analyzed by CellQuest and ModFit software (Becton Dickinson, San Jose, CA).

X-ray irradiation

Mice were irradiated with an MBR-1520R x-ray generator (Hitachi, Kashiwa, Chiba, Japan) mounted with a 1.0-mm aluminum filter. For cell count and thymocyte survival analysis, mice were irradiated at 0, 0.5, 1.0, 2.0, or 4.0 Gy and killed 21 hours after the irradiation. For cell cycle analysis, mice were irradiated at 0.5 Gy and killed 3 hours after irradiation. Thymocytes were collected, fixed with 70% of ethanol, and subjected to an analysis of DNA content.

Analysis of blood cells

Peripheral blood was collected from an axillary artery and promptly diluted with the same volume of PBS supplemented with 0.2% of EDTA-3K ([ethylenediaminetetraacetic acid]–3K). Densities of white blood cells, red blood cells, and platelets in peripheral blood were analyzed with a K-4500 hematology analyzer (Sysmex, Kobe, Japan). Surface marker molecules on peripheral white blood cells, thymocytes, and bone marrow cells were analyzed by means of an LSR flow cytometer (Becton Dickinson) after immunostaining with specific antibodies conjugated to fluorescent dye and treated with OptiLyse B reagent (Beckman Coulter, Hialeah, FL).

Transfection and establishment of stable transfectants of MEFs

Three cell lines of APEX2-null MEFs were transfected with pcDNA3.1/Hygro(+), pcDNA3.1/Hygro(+):mAPEX2, pIRES1hyg, or pIRES1hyg:mAPEX2 with the aid of LipofectAMINE (Invitrogen) according to the manufacturer's instructions, and stable transfectants were selected in the presence of 300 μg/mL hygromycin B. Expression of recombinant APEX2 protein was confirmed by Western blotting.

Colony formation assay

Exponentially growing MEFs were plated in 10-cm dishes at a density of 500 cells per dish. The cells attached to dishes by incubation for 6 hours were exposed to various doses of x-ray irradiation as described under "X-ray irradiation." Each plate was incubated for 2 more weeks. Formed colonies were stained in 25% ethanol containing 0.3% crystal violet, and counted.

Splenocyte proliferation assay

Splenocytes were prepared from 6-week-old male mice with an $Apex2^-$ or $Apex2^+$ genotype, treated with acetate kinase lysing buffer (pH 7.4, 150 mM NH_4Cl 10 mM KHCO3, 0.1 mM Na2-EDTA), and suspended in culture medium supplemented with 20 μg/mL lipopolysaccharide (LPS) (from *Escherichia coli*, 055:B5; Sigma, St Louis, MO) or 4 μg/mL concanavalin A (ConA) (Wako, Osaka, Japan) at a cell density of 1.0×10^6/mL. Then, 200 μL cell suspension per well was dispensed in multiple-well plates and cultured for 72 hours. Every 24 hours, the cells from 3 wells subjected to each treatment were harvested, and then viable and dead cells were stained by the trypan blue exclusion method and counted under a microscope.

For cell cycle analysis, 2 mL splenocyte suspension per well was dispensed in a 24-well plate. Cells cultured with LPS or concanavalin A were harvested at 48 hours and 60 hours, respectively. Nuclei were isolated from the harvested cells, and the DNA contents were analyzed as described.[14]

To analyze expression of APEX2 protein, 10 mL splenocyte suspension per dish was placed in 90-mm–diameter dishes (Nunc, Rochester, NY) for 48 hours, and cells were harvested. Whole-cell extracts were prepared and subjected to Western blotting with anti-mAPEX2.

Analysis of the immune response to chicken egg ovalbumin

Eleven-week-old wild-type (n = 6) and APEX2-null mice (n = 6) were immunized with 3 intraperitoneal injections of chicken egg ovalbumin (OVA) (Sigma) (300 μg per injection) on days 0, 21, and 35. Animals were separated into 2 groups, and on alternate weeks, peripheral blood was collected from the tail veins of each group in biweekly sampling. Concentrations of total immunoglobulin M (IgM), IgA, and IgG in serum were analyzed by the single radial immunodiffusion method,[16] and titers of OVA-specific antibodies were determined by an enzyme-linked immunosorbent assay using peroxidase-conjugated anti–mouse IgM (Rockland, Gilbertsville, PA) and anti–mouse IgG (Jackson ImmunoResearch Laboratories, Bar Harbor, ME) antibodies. Peroxidase activities were measured with a Sumilon peroxidase assay kit (Sumitomo Bakelite, Tokyo, Japan), according to the manufacturer's instructions.

Statistical analysis

To determine statistical significance, data of wild-type and APEX2-null mice were analyzed by the Welch *t* test, Mann-Whitney U test, or 2-way analysis of variance (ANOVA) with the use of StatView Software Ver. 5.0 (SAS Institute, Cary, NC).

Results

Growth retardation in APEX2-null mice

Heterozygous female (*Apex2*$^{+/-}$) mice bearing a mutated *Apex2* (*Apex2*$^{-}$) allele on an X chromosome, in which a genomic region from the 3′ region of its intron 5 to 5′ region of its exon 6 was replaced with a *neo* cassette,[14] were backcrossed with C57BL/6J males (*Apex2*$^{+/Y}$). From the backcross, almost equal numbers of wild-type (*Apex2*$^{+/Y}$) and knock-out (*Apex2*$^{-/Y}$) males, and wild-type (*Apex2*$^{+/+}$) and heterozygous females (*Apex2*$^{+/-}$) were obtained, indicating that the *Apex2* gene is not essential for viability (Table 1). The reverse-transcriptase polymerase chain reaction (data not shown) and Western blot analysis (Figure 1A) confirmed that thymocytes of *Apex2*$^{-/Y}$ mice are APEX2-null. The APEX2-null male mice showed moderate growth retardation (Figure 1B). Their body weights were about 80% those of the wild-type male littermates at birth, and this tendency persisted into childhood and adulthood (Figure 1C-D), indicating that all developing embryos, infants, and adults of APEX2-null mice may somehow be retarded in growth.

Thymic atrophy

Thymus glands of APEX2-null mice exhibited statistically significant atrophy, and their relative weights were about 50% those of the wild-type thymus (Figure 2A). The total number of thymocytes in APEX2-null thymus decreased to about 20% of that in the wild-type thymus (Figure 2B). Histologic abnormalities in the cortex or medulla of thymi from APEX2-null mice were not apparent, however, APEX2-null thymocytes appeared to be larger than the wild-type cells (Figure 2C). Flow cytometric analysis clearly showed that a fraction of small cells abundant in wild-type thymocytes, which is likely to represent the resting $CD4^+CD8^+$ thymocytes,[17] was largely reduced in the APEX2-null thymocytes (Figure 2D). Propidium iodide staining and flow cytometric analysis of isolated nuclei of thymocytes revealed that populations of APEX2-null thymocytes in both S and G_2/M phases were statistically significantly increased compared with the wild type (Figure 2E), indicating a delayed progression of S phase and increased arrest in G_2/M phase. APEX2-null female mice had essentially identical phenotypes, in terms of growth retardation and thymic atrophy, to those observed in APEX2-null male mice (data not shown).

General dyshematopoiesis

An analysis of peripheral blood cells of 6-week-old mice revealed general and moderate dyshematopoiesis in APEX2-null young mice (Table 2). The number of white blood cells in APEX2-null mice was significantly ($P < .01$) reduced to 42% of the wild-type level, and populations of $CD3^+$ T lymphocytes and $B220^+$ B lymphocytes were 44.8% and 33.3% of the wild-type levels, respectively, although the numbers of red blood cells, $CD11b^+$/$Dx5^-$ monocytes/granulocytes, $Dx5^+/CD3^-$, natural killer cells, but not platelets, were only slightly reduced (Table 2). We also

Table 1. Genotypes of progeny from backcrosses of heterozygous female (*Apex2*$^{-/+}$, F_1) with wild-type male (*Apex2*$^{+/Y}$, C57BL/6J) mice

Sex	Genotype, no.		
	WT	Heterozygous	KO
Male	13	0	15
Female	15	15	0

Heterozygous, *Apex2*$^{-/+}$; KO, *Apex2*$^{-/-}$ or *Apex2*$^{-/Y}$.

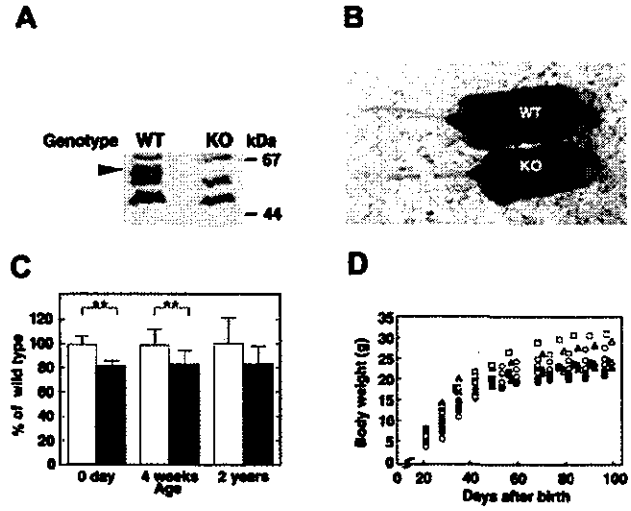

Figure 1. Growth retardation of APEX2-null mice. (A) No APEX2 protein was detected in the *Apex2* KO mouse. Whole-cell extracts of thymocytes from wild-type (WT) and *Apex2* KO mice were prepared. APEX2 protein in extracts was detected by Western blotting using anti-APEX2 antibody as indicated by an arrowhead. (B) Photograph of an F_6 15-week-old APEX2-null male mouse (KO) and its wild-type littermate (WT). Body weights of the KO and WT mice were 19.9 g and 27.2 g, respectively. (C) Mean values ± standard deviation (SD) of body weights of male mice with each genotype at an age of 0 days (F_{10} mice, 7 WT and 12 KO), 4 weeks (F_9 mice, 10 WT and 13 KO), and 2 years (F_3 mice, 12 WT and 7 KO) are shown. Open columns indicate WT; solid columns, KO mice. $^{**}P < .01$. No asterisk indicates not statistically significant ($P > .05$). (D) Growth curves of APEX2-null males and their wild-type littermates. Each symbol tracks the growth of an individual mouse. Littermates with different genotypes are indicated with the same symbol. Open symbols indicate WT; closed symbols, KO mice.

analyzed peripheral blood of 13-week-old adult APEX2-null mice, and observed decreased densities of white and red blood cells as compared with wild-type mice (Table 2). In thymus of 6-week-old APEX2-null mice, most fractions of thymocytes ($CD4^+CD8^+$, $CD4^-CD8^+$, and $CD4^+CD8^-$) were significantly ($P < .01$) reduced to about 20% of the wild-type levels (Table 3), as was observed in 4-week-old APEX2-null mice (Figure 2B). The number of $CD4^-CD8^-$ cells in the APEX2-null thymus was reduced to only 50% of the wild-type level. The relative ratio of $B220^+$ B cells in bone marrow cells was reduced to 75% of the wild-type level, irrespective of IgM expression (Table 4).

Sensitivity to x-ray exposure

After mice were exposed to 1 Gy x-ray irradiation, about 11% of thymocytes in APEX2-null thymus survived, while more than 41% of thymocytes survived in the wild-type mice (Figure 3A). The sub-G_1 fraction appeared in APEX2-null thymocytes 3 hours after the irradiation, but it was not so prominent in the wild type, indicating that APEX2-null thymocytes underwent apoptosis after x-ray exposure (data not shown). To examine whether the increased x-ray sensitivity of APEX2-null thymocytes is a general phenotype for any type of cells, we established immortalized MEFs from 3 APEX2-null embryos and introduced plasmid encoding mouse APEX2 protein to each cell line. Unexpectedly, each APEX2-null MEF line exhibited essentially the same colony-forming efficiency after exposure to various doses of x-ray irradiation, regardless of recombinant APEX2 expression (Figure 3B).

Abnormal proliferation and cell cycle progression of peripheral lymphocytes

To examine whether the defects observed in lymphopoiesis in vivo are cell-autonomous defects, we further analyzed cultured primary

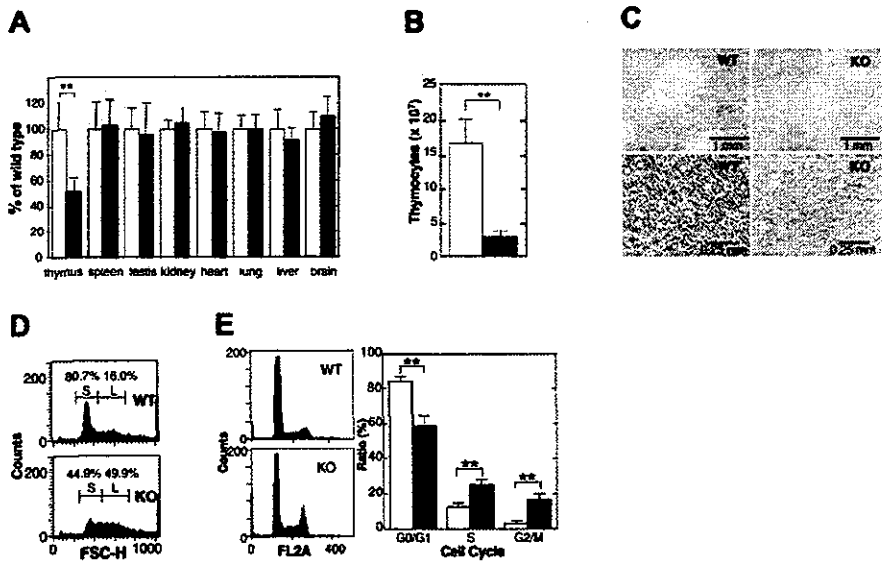

Figure 2. Thymic atrophy in APEX2-null mice. (A) Organ weight. The body weight and weight of each organ of 32- or 33-day-old F_7 male mice were measured, and the weight of each organ was normalized to the body weight of each mouse. The weight of each organ of APEX2-null mice (KO) was expressed relative to the weight of the corresponding organ of wild-type mice (WT) and shown as a percentage ± SD of the WT value. Open columns indicate WT (n = 11); solid columns, KO mice (n = 13). $^{**}P < .01$. No asterisk indicates not statistically significant ($P > .05$) (B) Total number of thymocytes. Means ± SD of the total number of thymocytes in thymus from 4-week-old male mice are shown. Open column indicates WT (n = 7); solid column, KO mice (n = 7). $^{**}P < .01$. (C) Histology. Thin sections of thymi of 4-week-old male mice were fixed with formaldehyde, embedded in paraffin, and stained with hematoxylin and eosin. Left panels are WT; right panels are KO mouse. (D) Flow cytometric analysis of thymocyte sizes. Thymocytes from WT (upper panel) and KO (lower panel) mice were analyzed by flow cytometry. Size distributions of thymocytes represented by forward scatter heights (FSC-Hs) are shown in histograms. Fractions of small and large thymocytes are indicated by S and L, respectively. (E) APEX2-null thymocytes show abnormal progression of the cell cycle. Isolated nuclei were stained with propidium iodide and cell cycle distribution was determined by flow cytometry. Left panels indicate representative histograms of DNA contents in isolated nuclei of thymocytes from WT (n = 7) and KO mice (n = 8). The distribution of isolated nuclei in each cell cycle phase was determined with the use of ModFit software and is shown with SD in the right panel. $^{**}P < .01$.

splenocytes. In the absence of stimulation, splenocytes isolated from both APEX2-null and wild-type spleen were mostly in the quiescent state, and similarly underwent cell death during in vitro culture (Figure 4A). After stimulation with either LPS or ConA, APEX2-null splenocytes started to proliferate, but the extent of proliferation was much less than in wild-type splenocytes. The number of dead cells in the culture of APEX2-null splenocytes was almost equal to that of wild-type splenocytes (data not shown). The relative ratio of APEX2-null cells in G_2/M phase was statistically significantly increased in comparison with the wild type (Figure 4B). Western blot analysis showed a notable induction of APEX2 expression in splenocytes after stimulation with these mitogens (Figure 4C).

Table 2. Moderate dyshematopoiesis in 6- and 13-week-old APEX2-null mice

Age of mice and cell type	Density, counts/μL*	
	Wild type	APEX2-null
6 wks		
WBC†	5400 ± 1095	2275 ± 640
RBC, ×10⁴‡	928 ± 41	771 ± 29
PLT, ×10⁴	60 ± 17	73 ± 25
CD11b⁺/Dx5⁻‡	877 ± 338	482 ± 154
Dx5⁺/CD3⁻	522 ± 151	391 ± 90
B220⁺†	3064 ± 513	1021 ± 308
CD3⁺†	1440 ± 344	643 ± 179
CD8⁺CD3⁺†	506 ± 109	227 ± 59
CD4⁺CD3⁺†	817 ± 150	345 ± 86
13 wks		
WBC†	6800 ± 748	3640 ± 804
RBC, ×10⁴†	945 ± 42	833 ± 29
PLT, ×10⁴	85 ± 24	105 ± 19

WBC indicates white blood cells; RBC, red blood cells; PLT, platelets,
*The mean ± standard deviation representing at least 5 mice.
†$P < .01$ by Welch t test.
‡$P < .05$ by Welch t test.

Attenuated immune response in APEX2-null mice

To evaluate the ability to produce functional antibodies, we initially analyzed levels of various immunoglobulins in peripheral blood of naive APEX2-null mice. Concentrations of total IgM, IgG, and IgA in peripheral blood of naive APEX2-null mice were essentially the same as in naive wild-type mice (Figure 5A). We then immunized APEX2-null and wild-type mice with OVA and collected peripheral blood from the immunized mice. From around 4 weeks after immunization, titers of anti-OVA IgM and IgG gradually increased in both APEX2-null and wild-type mice (Figure 5B); however, the mean titers of both anti-OVA IgM and anti-OVA IgG in the APEX2-null mice were always lower than those in the wild type, even at 7 weeks after the first immunization. We further immunized an additional 5 APEX2-null and 5 wild-type mice, collected their serum 4 weeks after the first immunization, and analyzed titers of anti-OVA antibodies. Although not of statistical significance ($P > .05$), mean titers of both anti-OVA IgM and anti-OVA IgG of

Table 3. Thymic dyslymphopoiesis in 6-week-old APEX2-null mice

Types of cells†	Cell count, ×10⁵ in thymus*	
	Wild type	APEX2-null
Total cells	1156 ± 125	234 ± 32
CD4⁻CD8⁻	45 ± 7	25 ± 5
CD4⁺CD8⁺	982 ± 128	179 ± 24
CD4⁻CD8⁺	33 ± 3	10 ± 3
CD4⁺CD8⁻	96 ± 8	20 ± 3
CD3⁺	88 ± 14	18 ± 3

*The mean ± standard deviation representing 5 mice.
†$P < .01$ by Welch t test.

Table 4. Decreased population of IgM⁻ B lymphocytes in 6-week-old APEX2-null mice

Type of cells	Percentage in bone marrow cells*	
	Wild type	APEX2-null
B220⁺†	35.2 ± 1.6	26.3 ± 2.2
B220⁺/IgM⁺	14.7 ± 2.2	12.2 ± 0.8
B220⁺/IgM⁻†	20.4 ± 1.4	14.1 ± 2.4

*The mean ± standard deviation representing 5 mice.
†$P < .01$ by Welch t test.

APEX2-null mice were consistently lower than those of wild-type mice, as shown in Figure 5C.

Discussion

APEX2 is highly expressed in mouse thymus, spleen, and bone marrow, consistent with the significant abnormalities in these organs seen in APEX2-null mice.[14] A major AP endonuclease, APEX1, is also highly expressed in these tissues; however, our results indicate that APEX2 deficiencies in these tissues are not compensated for by APEX1. Thus, results of the present study provide the first evidence for the biologic significance of APEX2 in mammals.

B lymphocytes were most severely reduced in peripheral blood of APEX2-null mice. Recently, it was reported that UNG-deficient mice and human patients exhibit abnormalities in immunoglobulin class-switch recombination and in somatic hypermutation in B lymphocytes.[18,19] Nilsen et al[20] reported the hyperplasia of lymphoid organs, including thymus in UNG-null mice; other mice deficient in any DNA glycosylase have never been reported to exhibit such hyperplasia of lymphoid organs. It has been shown that both UNG and APEX2 bind PCNA via their PCNA-binding motives, thus indicating that both play a crucial role during DNA replication or replication-associated BER.[4] It is most likely that lack of UNG results in reduced generation of AP sites while lack of APEX2 in the presence of UNG results in increased accumulation of AP sites. Thus, we suggest that the large number of AP sites in lymphoid cells cause dyslymphopoiesis as we observed in APEX2-null mice, and that dyslymphopoiesis may be suppressed by simultaneous loss of UNG. The fact that the major AP endonuclease, APEX1, could not efficiently compensate for the lack of APEX2 clearly demonstrates the biologic significance of APEX2, especially in lymphoid organs. The highest expression of some other DNA glycosylases, including MUTYH and NEIL3 (endonuclease VIII-like 3), were also detected in thymus.[1,21-23] MUTYH and NEIL3 have a PCNA-binding motif or a topoisomerase III homologous domain, respectively, which they shared in common with APEX2. Thus, we suggest that these DNA glycosylases may generate AP sites that are repaired by APEX2 in thymocytes. The difference in phenotypes of B lymphocytes and thymocytes may be due to accumulation of AP sites generated by UNG, MUTYH, NEIL3, or other DNA glycosylases. We did not observe any histologic abnormality in intestinal epithelium (data not shown), suggesting that the severely altered phenotype in APEX2-null mice is rather specific to lymphopoietic cells.

A decreased population of developing thymocytes as well as an abnormal proliferation of peripheral mature T lymphocytes was apparent in APEX2-null mice. Furthermore, various populations of

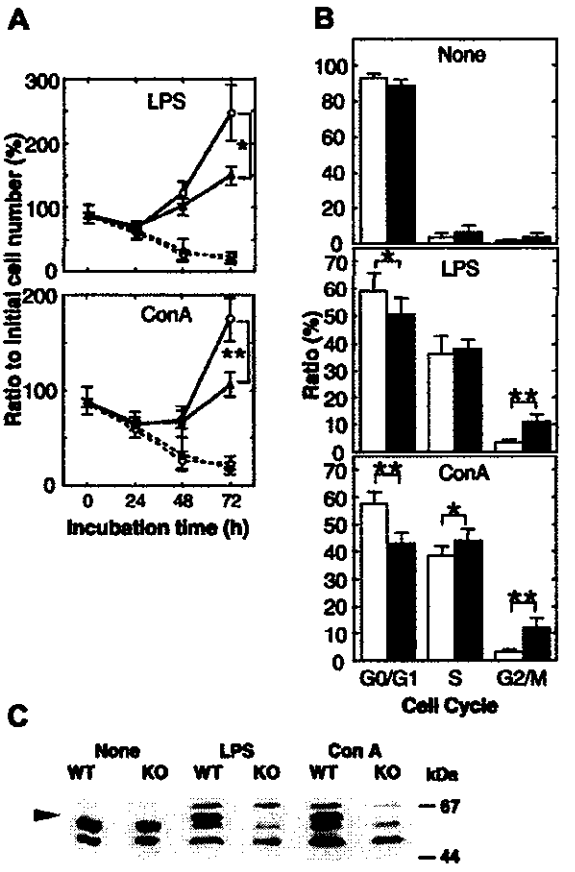

Figure 4. Delayed progression of the cell cycle during proliferation of peripheral lymphocytes. (A) Mitogen-induced proliferation of splenocytes of wild-type (WT, n = 4) and APEX2-null (KO, n = 4) mice. Splenocytes were stimulated with LPS or ConA, and numbers of viable cells were counted under a microscope. Mean values ± SD are indicated. ○ indicates WT; ▲, KO. Solid lines represent cells incubated with mitogens; dotted lines indicate that no stimulant was used. $^{**}P < .01$. $^{*}P < .05$. (B) Cell cycle distribution of proliferating splenocytes. DNA contents of isolated nuclei stained with propidium iodide were analyzed by flow cytometry. Distribution of isolated nuclei in each cell cycle phase is shown as a percentage ± SD. Open columns indicate WT (n = 7); closed columns, KO mice (n = 10). $^{**}P < .01$. $^{*}P < .05$. (C) Induction of APEX2 expression by stimulation with LPS or ConA for 48 hours. APEX2 protein in whole-cell extracts of splenocytes from WT and KO mice was detected by Western blotting using anti-APEX2, as indicated by the arrowhead.

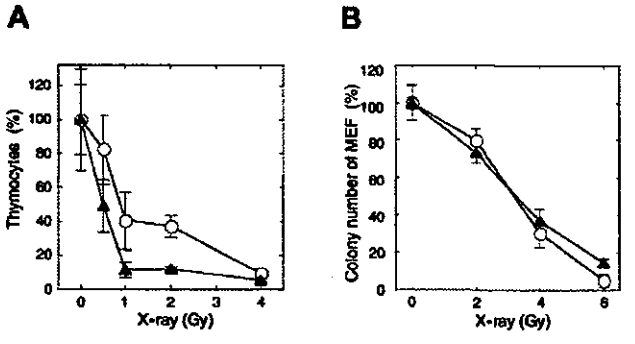

Figure 3. Increased sensitivity of thymocytes of APEX2-null mice to x-ray irradiation. (A) Mice were exposed to various x-ray doses. Thymus glands were collected 21 hours later, and viable thymocytes were counted. Ratios (percentages) of the numbers of thymocytes relative to those of an unirradiated control are shown with their mean values and SD. At least 3 mice were exposed to each x-ray dose. The difference between wild-type and APEX2-null mice was statistically significant ($P = .0006$, 2-way ANOVA). ○ indicates wild type; ▲, APEX2-null. (B) X-ray sensitivity of APEX2-null MEF lines. APEX2-null MEF lines with pIRES1hyg:mAPEX2 (○) or pIRES1hyg (▲) were plated in triplicate at a cell density of 500/10-cm dish and exposed to x-ray irradiation. After culture for 14 days, colonies were stained with crystal violet and counted. Ratios (percentages) of the numbers of colonies relative to those of an unirradiated control are shown with their mean values and SD.

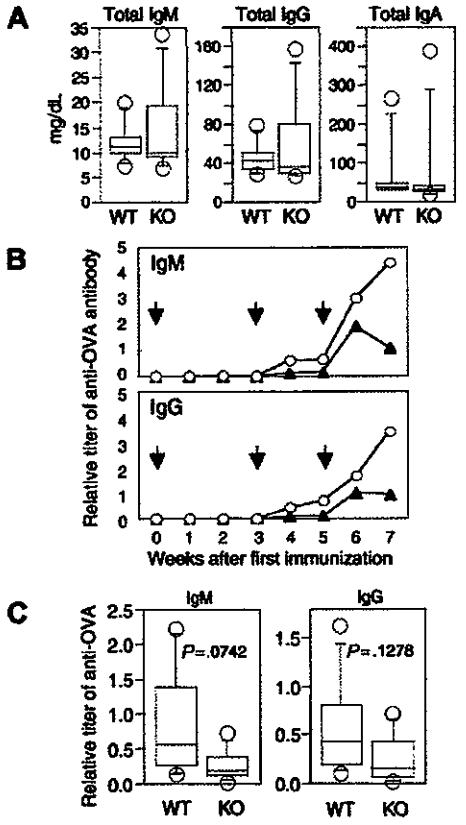

Figure 5. Immunoglobulin levels in peripheral blood of naive and immunized APEX2-null mice. (A) Concentrations of IgM, IgG, and IgA of 11-week-old naive wild-type (WT, n = 7) and APEX2-null mice (KO, n = 8). Concentrations of immunoglobulins in serum are shown with box-and-whisker plots. In each plot, the box is bound top and bottom by upper and lower quartiles, and the statistical median is shown as a horizontal line within the box. The whiskers extend outward from the box to the farthest points that are not outliers (circles). The concentration of each immunoglobulin (IgM, IgG, or IgA) in serum of APEX2-null mice was not significantly different from that of wild-type mice (Mann-Whitney U test, $P > .05$). (B) Time-dependent induction of antigen-specific antibodies in wild-type and APEX2-null mice after immunization with OVA. Eleven-week-old wild-type (n = 6) and APEX2-null (n = 6) mice were immunized with 300 μg OVA on days 0, 21, and 35 as shown by arrows. Animals were separated into 2 groups, and serum was collected biweekly from each group of mice on alternate weeks. The mean titers of anti-OVA IgM and IgG of wild-type mice (○) and APEX2-null mice (▲) are shown as line graphs. (C) OVA-specific antibodies in wild-type and APEX2-null mice immunized with OVA for 4 weeks. A total of 8 mice were immunized with OVA as described in panel B. The titers of their serum anti-OVA IgM and IgG are shown with box-and-whisker plots. Differences between wild-type and APEX2-null mice were not statistically significant (Mann-Whitney U test, $P > .05$).

hematopoietic lineages, which are derived from common stem cells in bone marrow, were significantly decreased in peripheral blood of APEX2-null mice. Thus, our data may suggest that there is an attenuated proliferation of bone marrow stem cells as well as abnormality in peripheral mature blood cells of APEX2-null mice.

Using spontaneously immortalized or simian virus 40 (SV40) T antigen-immortalized APEX2-null MEF lines, we analyzed their sensitivity to various DNA-damaging agents such as hydrogen peroxide, bleomycin, or x-ray irradiation; however, any protective effect of endogenous APEX2 in wild-type MEF lines or recombinant APEX2 protein expressed in all APEX2-null MEF lines was not evident (Figure 3B; also D.T., Y.I., Y.N., unpublished results, December 2002). Furthermore, after hydrogen peroxide challenge, we did not observe any difference in survival between APEX2-null and wild-type mouse embryonic stem cell lines.[14] Thus, it is likely that APEX1 but not APEX2 plays major role in base excision repair against such DNA damaging agents in these cell lines, suggesting that APEX2 function is selectively required for proper cell cycle progression of activated T cells and B cells. The increased population of proliferating lymphocytes in both S and G_2/M phases in APEX2-null mice suggests that an APEX2 deficiency increases the obstacles to be overcome for progression of the cell cycle. APEX2 but not APEX1 would be required in replication-associated BER to incise AP sites in the nascent strand because of the ability of APEX2 to bind PCNA. Thus, the lack of APEX2 most likely results in a delayed progression of replication-associated BER. We hypothesize 2 models for a mechanism of replication-associated BER. The first is a replication-coupled BER, in which misincorporated bases such as uracil or adenine opposite 8-oxoguanine are repaired immediately after their incorporation by replicative DNA polymerases. The other is a postreplicative BER, in which misincorporated bases left behind replication forks are repaired before completion of S phase. In either model, the inefficient PCNA-anchored BER machinery itself might be an obstacle to DNA replication and cause delayed S phase and G_2/M phase arrest. We did not detect any increased apoptosis in thymocytes and stimulated splenocytes, and this may indicate that the remaining AP sites in APEX2-null cells are likely to be slowly repaired by APEX1. It has been reported that *Saccharomyces cerevisiae* also possesses a APEX2 homolog, Apn2.[24] Recently, Guillet et al[25] reported that an *S cerevisiae* mutant strain lacking *apn1*, *rad1*, *ung1*, and *apn2*, which possesses decreased AP endonuclease activities, exhibits growth delay owing to a G_2/M checkpoint arrest. Our data observed in APEX2-null mice are in good agreement with the phenotype.

After immunization with OVA, production of anti-OVA antibodies in APEX2-null mice was somehow retarded in comparison with wild-type mice. Notably, anti-OVA IgG was apparently induced in APEX2-null mice as well as anti-OVA IgM, indicating that immunoglobulin class-switch recombination (CSR) was achieved. UNG, in addition to its general role in replication-associated BER, is thought to play a specific role in CSR by excising the uracil base produced by activation-induced cytidine deaminase (AID).[18,19] This function of UNG might be independent of PCNA because generation of uracil base in DNA by AID should be independent of DNA replication. APEX2 is the PCNA-associated AP endonuclease, and thus may participate in replication-associated BER initiated by UNG or other DNA glycosylases, but not in the AID-initiated CSR during which UNG produces AP sites independent of PCNA.

An APEX2 deficiency in mice is not lethal and may be associated with certain human hereditary diseases. The human *APEX2* gene is also located on the X chromosome[9]; thus, a mutation in one *APEX2* allele of a germ line might easily lead to the birth of APEX2-deficient male offspring. The human diseases anticipated from an APEX2 deficiency might be more prevalent in males and be associated with decreased body size, moderate immunodeficiency, and a high sensitivity of lymphocytes to x-ray irradiation.

Acknowledgments

We thank M. Furuichi and H. Sumichika for their helpful discussions; A. Matsuyama, S. Kitamura, J. Ikeda, and Y. Yamada for their technical assistance; and W. Campbell for comments on the manuscript.